Received: 26 August 2021 | Revised: 12 December 2021 | Accepted: 14 December 2021

DOI: 10.1002/eqe.3598

RESEARCH ARTICLE

WILEY

Damping considerations for rocking block dynamics using the discrete element method

Francisco Galvez[1] | **Luigi Sorrentino**[2] | **Dmytro Dizhur**[1] | **Jason M. Ingham**[1]

[1] Civil and Environmental Engineering Department, University of Auckland, Auckland, Aotearoa, New Zealand

[2] Deparment of Structural and Geotechnical Engineering, Sapienza Università di Roma, Roma, Italy

Correspondence
Francisco Galvez, Civil and Environmental Engineering Department, University of Auckland, Auckland, Aotearoa New Zealand.
Email: fglv390@aucklanduni.ac.nz

Funding information
QuakeCoRE

Abstract

It is well established that unreinforced masonry (URM) buildings develop damage-forming collapse mechanisms during high-intensity earthquakes, with these mechanisms exhibiting large rocking displacements before collapsing. The Discrete Element Method (DEM) of analysis can realistically capture phenomena that involve large movements of elements, resulting in the technique being ideal for simulating the collapse of URM building elements. Consequently, extensive research using DEM to analyse the seismic response of URM buildings and building components has recently been published. However, the variety of reported damping approaches that have apparently led to DEM results that successfully replicate physical observations underscores the need for consistent guidance related to the assignment of damping factors. The Rayleigh damping distribution model implemented in the DEM software 3DEC was used to study the differences between mass proportional (MP) and stiffness proportional (SP) damping configurations. After reviewing phenomena that need to be damped and previous works where damping was implemented, the capabilities and drawbacks of the time-efficient MP damping configuration were studied and the results compared to simulations with SP damping. When considering numerical simulations that incorporated MP damping and led to results that were seemingly well-matched to experimental tests, it was found that the apparent robustness of decisions pertaining to the adopted input parameters was deceptive in most cases. Consequently, SP damping was recommended for all DEM rocking simulations, even though MP damping could be used with satisfactory accuracy in certain situations discussed herein. A pragmatic relationship between both damping strategies was proposed.

KEYWORDS
collapse mechanisms, discrete element method, Rayleigh damping, rocking, seismic simulation, unreinforced masonry

1 | INTRODUCTION

It has been demonstrated that the discrete element method (DEM) is a suitable strategy to investigate and predict the complex dynamic behaviour of rocking structures such as bridge piers, nuclear reactors, hospital cabinets, soil-foundation-structure interaction, historic monuments, and unreinforced masonry (URM) parts when subjected to earthquake-induced shaking.[1–7] DEM was first presented by Cundall[8] and later extended using a 3D version[9] originally conceived for jointed rock simulations. One of the principal strengths of using DEM is the ability to simulate large relative displacements between elements. Complete separation between elements that were previously in contact may happen and new contacts can be formed, allowing the modelling of the dynamic collapse behaviour of complex structures.

Explicit time-stepping algorithms are commonly used for DEM where the equations of motion are integrated using a central-difference scheme.[10,11] The same algorithm is often used for quasistatic and dynamic simulations, overdamping the kinetic energy of the system in the quasistatic case by applying viscous damping forces to each element. Rayleigh damping is commonly used to account for energy losses in dynamic simulations and is described by two components, being damping proportional to mass (MP) and damping proportional to stiffness (SP).[12] MP damping consists of the application of a force resulting from the product of absolute velocity of the block, mass of the block, damping ratio and rotational frequency, with direction opposite to the velocity vector. This type of damping decreases non-linearly with increasing frequency, resulting in plausible damping ratios for higher frequency motions but producing an overdamped response at low frequencies that potentially leads to artificially restricted motion of the blocks. Thus, MP damping is generally not recommended for problems that involve large displacements of blocks, which implies low-frequency oscillations.[11,13] Alternatively, when the phenomena to be modelled imply high-frequency oscillations, the SP component of Rayleigh damping is desirable in order to avoid non-realistic behaviour.[14] However, the computational time of certain problems may then become impractically long because the application of SP damping requires a time step that is smaller than that required by the conditionally stable explicit scheme. Another factor that makes for lengthy computation time when using SP damping is the required number and size of the discrete elements.

In the presented study URM was used as a representative material for elements that rock when subjected to earthquakes. It was not until the 1990s when DEM was first used to simulate URM structural performance when considering the dynamic response of columns and arches of Greek classical temples subjected to strong earthquake motions.[13,15–17] Since then, several authors have successfully simulated the dynamic behaviour of URM buildings when subjected to earthquake-induced shaking.[12,18–22] In a DEM simulation each masonry unit can be individually represented as a rigid or deformable element and the joints between the units are modelled as interfaces (referred to as a meso-modelling approach as per Lourenço[23]). Alternatively, a set of adjacent units are combined into a single element in order to reduce the computational burden.

For the case when simulating the behaviour of URM walls using discretised strategies to model every real unit (or brick) as a single block, several authors have encouraged the use of no viscous damping, instead relying on the frictional energy dissipation effect and bond breakage[21,24] to obtain reasonable results. Another possible option is to damp the fundamental frequencies of the structure by applying the desired damping ratio (generally 5%) at these frequencies, whilst having minimal impact on the rocking frequencies. In the presented study a discretised non-damped strategy for rocking was included and the influence of joint properties on the rocking motion was discussed. This non-damped strategy was implemented by Forgács et al.[6] for complex configurations using DEM, where soil-structure interaction was also included. When simulating structures built with large blocks, and with no cohesive layer between them, multiple authors[21,25–27] have relied on frictional energy dissipation while others[1,3,28,29] have used viscous damping to damp high-frequency impacts. DEM can also be applied to simulate in-plane loading in discretised URM walls as done by Malomo et al.,[30] where interfaces within the blocks were included to allow for brick cracking. Research has been undertaken on the effects of interface material on the performance of free rocking blocks[29,31,32] representing façades or mechanisms that have contact with the foundation, with the conclusion being that damping parameters can be estimated based on the material properties of the rocking block, and that changing the stiffness of the interface between the foundation and block will suffice to capture soil-structure interaction effects.

Considering the numerous options for the application of damping and the multiple factors that influence the results described above, one can find it challenging to choose a correct damping approach with sufficient confidence. It was found that several authors have previously assigned damping values without a thorough discussion when using DEM dynamic simulations, probably due to a lack of explanatory literature available on the topic. In some cases, authors generated fragility curves that most likely contained errors because the damping option chosen was not appropriate for the phenomena being modelled, instead validating their models by fitting values using trial and error iterations that gave artificial support of good correlations.

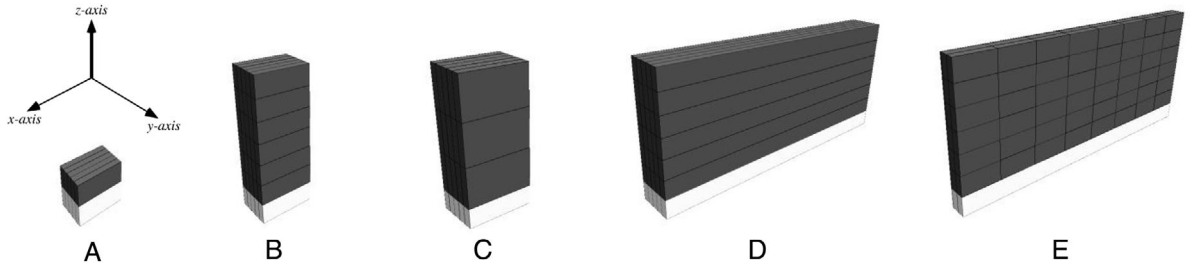

FIGURE 1 Block geometries and variations of discretisation for measurement of rattling (Light coloured block represents fixity)

In an attempt to establish guidance to support future modelling research, a comprehensive literature review of previously adopted damping strategies applied to DEM simulations of URM buildings and building parts was included herein. This review serves as an aid to allow the reader to gain an awareness of the problems that will be encountered when attempting to model rocking using DEM. Rayleigh damping applied to dynamic DEM simulations for rocking blocks was comprehensively studied. Such rocking blocks represent collapse mechanisms triggered by out-of-plane forces, where damage through the bricks that form the wall is unlikely to occur and only mortar crushing at the bottom edges is expected.[29] After studying common issues to be aware of when using Rayleigh damping in DEM, experimental testing results reported in the literature were compared to the results of a DEM model reported herein. Sources of error and issues that were identified in the application of viscous damping are reported, together with lessons learnt and recommendations for future studies. The various issues encountered when applying MP damping were investigated by performing parametric analyses and simulating laboratory tests. In the reported study only rigid elements were used, with deformations localized at the interface joints. The numerical and physical phenomena that need to be damped to avoid errors when computing the rocking motion of blocks in DEM were also studied.

2 | PHENOMENA TO DAMP IN SIMULATED ROCKING MOTION

Incorrectly damping high frequencies causes motion that is not compliant with the mechanics of rocking blocks, potentially resulting in undesired sliding, loss of solution accuracy,[33–35] or premature collapse as studied empirically and numerically by Meyer et al.[36] Two types of undesired high-frequency displacements must be damped in DEM rocking simulations: (1) high-frequency numerical noise, known as the "rattling effect"[26,37–39]; and (2) the rebound effect caused by a block impacting the ground or other blocks.

2.1 | "Rattling Effect": High frequency numerical noise

With the aim of better understanding the rattling effect, vertical and horizontal displacements caused purely by numerical integration were investigated for a range of squat structures with cohesive connections, including a fixed block at the ground, with the joint location and block shapes varied as seen in Figure 1. In order to measure the displacements occurring due to rattling, the blocks were subjected to free vibration with no external input other than gravity. Frequencies of vibration of between 300 Hz and 1600 Hz, calculated as the inverse of the measured complete noise oscillations per second, were observed for URM columns made out of two and seven blocks having block dimensions of L370 × W250 × H120 mm^3 in size (Figure 1A,B), with the number of blocks in the column altering the vertical amplitude of the rattling from 2e-4 mm (two blocks) to 22e-4 mm (seven blocks). Increasing the height of the blocks whilst maintaining a constant column height and constant Young's modulus of $E = 1800$ MPa (Figure 1B,C) led to a reduction of both amplitude and frequency of the rattling. Horizontal rattling was also observed in models a, b and c but the amplitude was in the order of 1e-17 mm. Conversely, changing the length of the blocks did not change the rattling response (Figure 1B,D), leading to the conclusion that the taller the structure, the greater the vertical rattling amplitude and the lower the rattling frequency. When vertical joints (and hence additional integration points and additional degrees of freedom) were included in a wall having the same material properties and characteristics as the columns (Figure 1D,E), rattling displacements increased in the vertical direction (z) and in the direction perpendicular to the length of the wall (y). For a seven-block tall wall (Figure 1E) the displacement reached 4e-3 mm in the y-direction and 1e-3 mm in the z-direction. Increasing the height of the wall from 0.84 to 3.00 m increased the vertical rattling amplitude, confirming the phenomena reported above for the URM columns.

However, after a few seconds of simulation, a joint at the bottom of the wall failed and the wall suffered a drift of 14e-3 mm, leading to the conclusion that the rattling effect can lead to unrealistic failure of joints, usually due to tensile failure of the bottom bed-joint. When a cohesionless bottom bed-joint was used in the macroblocks the seven-block wall had a vertical rattling displacement of 3e-4 mm, which was a lower value than that observed with a cohesive base (4e-3 mm) that consisted of an interface with cohesion $c = 1.4$ MPa, tensile strength $f_t = 0.84$ MPa, and friction coefficient $\mu = 0.7$. Rattling oscillations in the bricks happen because joints allow for movement of their nonlinear springs governed elastically by normal and shear stiffness. Columns and walls with the same block configuration will experience higher rattling effect with lower stiffness.

2.2 | Impact frequency

At the onset of the rocking motion the block rotates about one edge until eventually impacting with the ground and completing half of an oscillation, then rebounds and continues rocking around either the same or the opposite edge. While bouncing is an expected high-frequency response of URM rocking motion, this response is generally damped in nature.[40–42] Therefore, the same damped bouncing motion has to be considered when numerically simulating the rocking problem and critically damping the impact frequencies by using SP damping. The application of SP damping to the critical frequency was thoroughly studied by DeJong[43] who described three types of impacts for a 2D rocking block, and defined each type related to a 2D DEM model with spring-dashpot elements at each corner-edge or corner-corner contact.

The three types of impacts studied by DeJong[43] were: corner (edges in 3D), edge (surface in 3D), and rotational impact, with a circular frequency assigned to each impact type (ω_c, ω_e, ω_r, respectively) based on the stiffness and the mass assigned to the sub-contact springs in the contact. The special case of rotational impact can only occur when the block is subjected to external excitation, because this type of impact involves rotation about one corner, impact against the ground, and finally, rotation about the same corner. Due to the stretch rule, the rocking motion of a block remains unchanged if the block is stretched parallel to the axis of rotation such that the impact frequencies of a 2D and a 3D block remain the same. The formulation is recalled herein as:

$$\omega_c = \sqrt{\frac{k_s}{m_b}} \qquad \omega_e = \sqrt{\frac{2 \cdot k_s}{m_b}} \qquad \omega_r = \sqrt{\frac{3 \cdot k_s \cdot B^2}{m_b \left(B^2 + H^2\right)}} \tag{1}$$

where k_s is the stiffness of a spring at the contact surface, m_b is the mass of the block for 1 m length, B is the length of the base of the block and H is the height. For rigid block simulations, all deformations are lumped at the contact surface. Hence, the stiffness of the block (k_j) can be related to a spring stiffness on the joint (k_s) and to the material properties as:

$$k_j = \frac{E \cdot B}{H} \qquad k_s = \frac{k_j \cdot B}{2} = \frac{E \cdot B^2}{2 \cdot H} \tag{2}$$

where k_s was multiplied by $B/2$ as a consequence of having two springs positioned at the opposite ends of a joint. Substituting Equation 2 into Equation 1, the impact frequency relationships are:

$$\omega_c = \sqrt{\frac{E \cdot B^2}{m_b \cdot 2 \cdot H}} \quad \omega_e = \sqrt{\frac{E \cdot B^2}{m_b \cdot H}} \qquad \omega_r = \sqrt{\frac{3 \cdot E \cdot B^3}{2 \cdot H \cdot m_b \left(B^2 + H^2\right)}} \tag{3}$$

DeJong[43] observed little difference in the response of a rocking block when subjected to sinusoidal input when either ω_c, ω_e, or ω_r was selected as the critical frequency (ω_{crit}) to define critical damping. Hence, the highest frequency should be used to obtain β (stiffness-proportional damping parameter further defined in Section 3) in order to affect the timestep as little as possible. Because DeJong[43] demonstrated that the non-equivalence $\omega_r < \omega_c < \omega_e$ is true provided that $H/B > \sqrt{2}$, which is the case for most URM collapse mechanisms, ω_e was chosen herein as the critical damping frequency to ensure a correctly damped simulation while still having the largest possible timestep. Recent work by Mehrotra and DeJong[29] simulated multiple blocks in a post-and-lintel rocking frame configuration having multiple different ω_r and ω_e in the system. The authors found that by choosing the highest ω_e as the critical frequency the edge impacts and rotational impacts of some blocks were excessively underdamped. Thus ω_r was chosen as the critical frequency for a better redistribution of damping across the system.

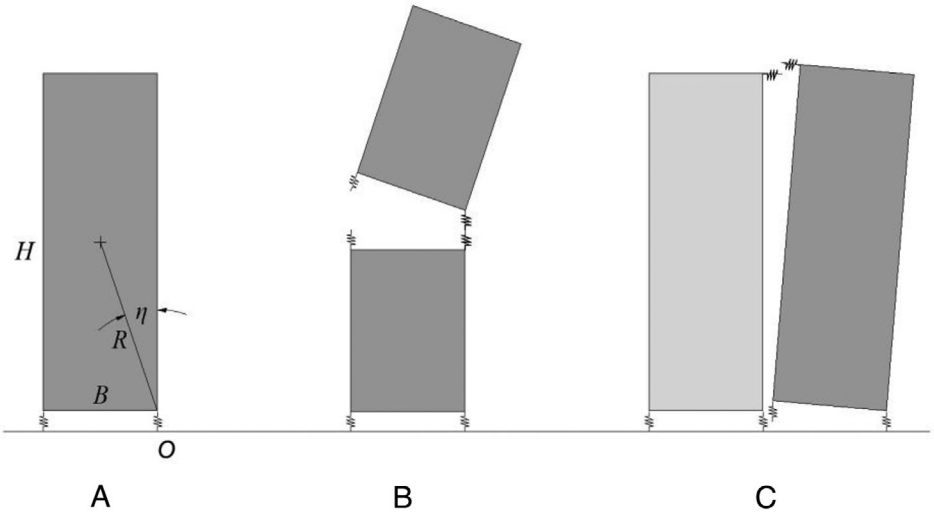

FIGURE 2 Diagram of rocking interacting blocks (Light coloured block represents fixity). (A) Single block, (B) (Vertically) Stacked blocks and (C) (Horizontally stacked) One-sided block.

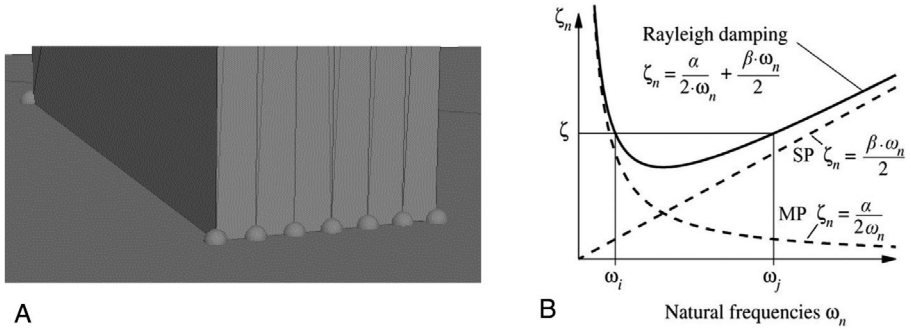

FIGURE 3 Block sub-contact representation and damping model distribution. (A) Block interface integration points with sub-contacts represented as spheres and (B) Variation with frequency of the MP, SP and Rayleigh damping models (adapted from Chopra[56]).

When simulating the rocking interaction of various stacked blocks having coinciding corners (see Figure 2B), the stiffness of the sub-contact at the corner of the blocks is effectively lumped into an equivalent spring with double the stiffness. Applying this increment of stiffness into the frequency calculation, DeJong[43] concluded that the critical frequency for interacting blocks could be estimated as ω_{crit} from Equation 3 times $\sqrt{2}$. In the special case of a one-sided rocking (1SR) block (Figure 2C) the combination of interacting springs is equal to the single rocking block (Figure 2A) during most of the rocking time except when the wall impacts the return walls, which corresponds to a horizontally stacked block configuration (Figure 2B). For horizontally stacked blocks the same formulation can be used as for vertically stacked blocks, except B would be H and vice versa, resulting in a significantly higher ω_{crit} for $H/B > \sqrt{2}$. In the DEM software 3DEC only one damping-related value can be input for a simulation, which corresponds to a single critical frequency. The use of ω_{crit} for horizontally stacked blocks results in underdamping for most of the simulation except for impact with the return wall. On the contrary, the use of ω_{crit} for a single rocking block overdamps the return wall impact. This damping issue is further studied in Section 4.2.

3 | DAMPING STRATEGIES FOR DEM AND INFLUENCE ON OUTCOMES

Several authors have suggested that MP damping could overdamp low frequencies due to the damping distribution, as seen in Figure 3B for frequencies lower than ω_i. However, many authors have performed successful dynamic simulations using an MP damping approach in 3D disregarding the drawbacks and achieving reasonably good matches with experimental observations and with favourable computational time.[16,19,44] Psycharis et al.[45] and Çaktı et al.[46] also used MP damping to perform incremental dynamic analyses[47] to study the specific behaviour of an URM part of a building.

In both studies[45,46] the fact that high frequencies would be underdamped in order to reduce the computational effort was acknowledged. Other authors decided to disregard damping in 2D[21,25] and 3D[7,26,27] problems when simulating rocking motion, by instead relying purely on frictional dissipation. Zero damping was assumed during the first 20 s of the excitation in Psycharis[48] and Psycharis et al.,[24] which was sufficient to capture the duration of significant shaking of the earthquake. After twenty seconds of shaking MP damping was applied to attenuate free rocking oscillations and adequately estimate the residual drift. The use of zero damping was justified by the observations of Psycharis et al.,[25] who demonstrated that the earthquake rocking response of free-standing blocks was independent of the value of damping except for the case when free rocking oscillations occur. Other researchers sometimes used SP damping together with MP damping for 2D simulations[13,21] and 3D simulations,[22,49] recognising the time-intensive nature of the problem. In addition to the reviewed DEM simulations, FEM models that applied MP damping[50] and SP damping[51] were found to correlate well with experimental rocking observations. Due to the high quantity and the variety of well-matched simulations to experimental testing using MP ($\beta = 0$) damping, SP ($\alpha = 0$) damping, a combination of both forms of damping, or zero damping, one can find it challenging to choose a correct damping approach for an URM simulation.

The only references in the literature for assigning damping parameters to rocking blocks are DeJong,[43] as described in Section 2, and Peña et al.[52] Both authors recommend using SP damping and leaving α as zero, but without exploring the possibilities, advantages, and disadvantages of using MP damping. Peña et al.[52] developed an empirical correlation between the coefficient of restitution (e), as an impact velocity reduction coefficient, and β via a generalised damping factor (GDF) where GPF is dependent on the stiffness of the block. If the formulation given by Peña et al.[52] to calculate the block stiffness is applied, then an extremely low contact stiffness is obtained which subsequently leads to numerical instability in the simulations. Conversely, DeJong[43] recommended that the contact stiffness be calculated as the relationship between the distributed load applied normal to the interface (σ_n) and the displacement produced by the load (u_n). A relationship between URM mechanical properties and the interface stiffness can be derived as $k_n = \sigma_n/u_n = E \cdot \varepsilon_n/u_n = E \cdot u_n/u_n \cdot l = E/l$, where u_n is the normal displacement of the joint, ε_n is the normal strain of the block, and l is the joint spacing, which for a single block representing an URM wall is equal to H and for a wall with n_b blocks is $l = H/n_b$. While in Equation 2 the spring stiffness was computed with reference to the block stiffness to obtain the impact frequencies, here the logic behind how to obtain the interface stiffness was recalled. Using elastic relations k_s can be calculated from k_n as $k_s = k_n/2 \cdot (1 + \upsilon)$, where υ is the Poisson ratio which was taken in this study as 0.25, resulting in the equation $k_s = 0.4{\cdot}k_n$. In the following sections of the reported study, k_n, k_s and G were not included unless strictly necessary because E was systematically stated and k_n and k_s can be computed based on the provided equations applying the chosen l. Stresses calculated along the nonlinear joint interface were modelled using the Mohr-Coulomb failure criterion with tension cut-off and a shear stress limit. The interface material model offers the option of including dilatancy, but variation of this parameter does not influence the presented results because the simulated out-of-plane rocking motion does not include overburden. Therefore, dilatancy was not reported.

Recent research has correlated the coefficient of restitution (e) of a two-sided rocking block and ζ_n in an analytical viscous damping model,[53] based on the solution of the piece-wise formulation of the equation of motion of a SDOF spring-mass model. Following this study, Vlachakis et al.[51] expanded the correlation for two-sided and one-sided rocking blocks using numerical finite element method models, which included contact surfaces between blocks and boundaries. The correlation was suggested to be applicable to multiple numerical approaches provided that an accurate estimation of e is achieved.

Because rocking problems cannot rely on hysteretic damping, a viscous approach already implemented in 3DEC was used in order to damp the phenomena described in Section 2. Viscous damping forces that are proportional to relative velocities simulate the effect of dashpot elements at each corner of blocks in contact (sub-contacts, see Figure 3A) following the Rayleigh damping criteria. Rayleigh damping makes use of the constants α (MP) and β (SP) to construct the damping matrix when performing dynamic analysis. The damping ratio ζ_n for any circular frequency ω_n that results from the application of α and β can be found in Bathe and Wilson[54] as:

$$\zeta_n = \frac{\alpha}{2 \cdot \omega_n} + \frac{\beta \cdot \omega_n}{2} \tag{4}$$

reaching a minimum at:

$$\beta = \frac{\zeta_{min}}{\omega_{min}} \qquad \alpha = \zeta_{min} \cdot \omega_{min} \tag{5}$$

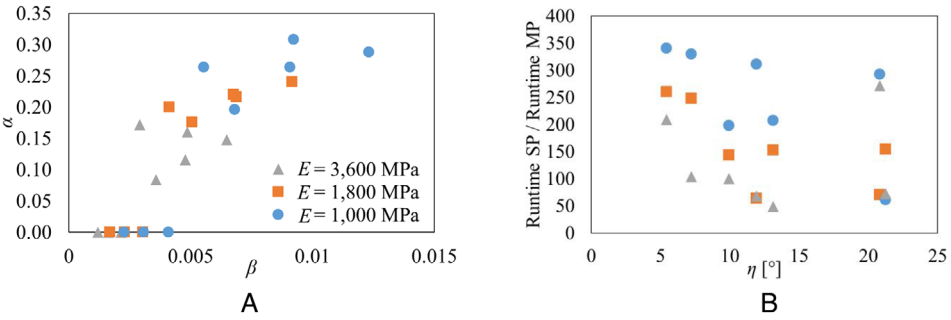

FIGURE 4 Run times of simulations with seven different geometries and with SP and MP damping. (A) Comparison between α and β and (B) Ratio between SP damping runtimes and MP damping runtimes.

Once the value of ω_{crit} is selected, β can be easily calculated with Equation 5. If Equation 4 is plotted as in Figure 3B it can be identified that the MP damping ratio distribution decreases hyperbolically with frequency and that the SP damping ratio increases linearly with frequency, with the final Rayleigh curve depicting a trough of damping ratios between frequencies ω_i and ω_j (see Figure 3B). Experimental observations of a distribution of damping ratios that are similar to the Rayleigh damping distribution in vertically spanning URM rocking walls can be found in Lam et al.,[55] who successfully implemented Rayleigh damping into a single degree of freedom analytical model to replicate experimental rocking tests.

As previously mentioned, when using MP damping there is a risk of overdamping low frequency motion associated with high amplitude rocking. In a possible scenario where the MP damping parameters are adjusted such that low frequency motions receive just the appropriate amount of damping, higher frequency motions would remain effectively underdamped due to the shape of the MP damping distribution (Figure 3B). Taking into account this drawback, the MP damping approach was studied in comparison with the SP damping approach because of the encouraging well-matched results of some research studies where MP damping was adopted.

In order to achieve numerical stability of DEM simulations, the required timestep Δt is calculated in relation to the mass of the smallest block (m_{min}) and the maximum contact stiffness of the model (k_{max}) as $\Delta t = 0.2\sqrt{m_{min}/k_{max}}$.[11,20,37] By specifying SP damping, the timestep is automatically further reduced for numerical stability, and a new timestep is calculated as specified in Itasca[11] and Belytschko.[57] During the simulation of rocking phenomena new contacts are created and bond breakage occurs, causing differences in calculation time due to having more phenomena to solve while keeping the timestep constant.

3.1 | Pragmatic differences between SP and MP damping applied to free rocking blocks

In order to compare computation time and investigate the pragmatic differences between the MP and SP damping approaches, eight single block geometries (see Figure 2A) using two fixed values of B (0.19 m and 0.35 m) while changing the values of H (0.5 m, 0.9 m, 1.5 m, and 2.0 m) were modelled with two contact points in order to identify a model that is numerically efficient if a large number of simulations need to be performed. The same modelling strategy was followed in all simulations reported hereafter. Further investigation on the influence of integration points in rocking block dynamics is discussed in Section 3.3. Two simulations were developed for each geometry, with one simulation incorporating SP damping and the second simulation incorporating MP damping. First, the DeJong[43] recommendations were followed to assign β (considering E as 1000 MPa, 1800 MPa, and 3600 MPa) and a free rocking test was performed from an initial tilting displacement of 90% of the instability displacement. Secondly, the best fitting α (MP damping approach) to match the SP damping simulation was chosen by obtaining the minimum Weighted Mean Error (WME) between the displacement time-history results of both models (same procedure as in Shawa et al.[58]). This WME represents the mean difference between the displacement obtained in the simulations using SP and using MP damping over the duration of the free rocking, with a cut-off at the end time of the SP damping simulation (displacement practically equal to zero) to not account for undamped high-frequency low amplitude oscillations of the MP damping simulation. Figure 4A shows the regression relationship between α and β for free rocking and in Figure 4B the ratio between the runtime of the simulations with SP damping and with MP damping can be observed ($\eta = \tan^{-1}(B/H)$, Figure 2A). A coarse correlation was obtained in Figure 4A, where for similar β different α were obtained, mainly due to two factors. First, according to Equation 3 blocks

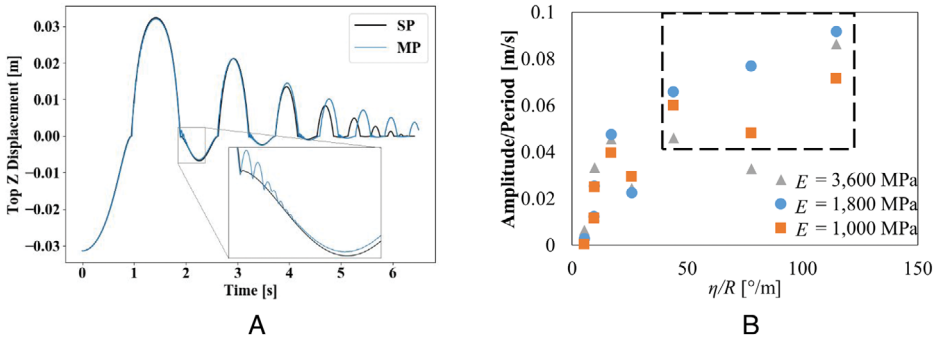

FIGURE 5 Bouncing observations. (A) Observation of bouncing in the MP simulation of the block with 0.35×1.50 m^2 dimensions and $E = 3{,}600$ MPa and (B) Relationship between block dimensions and observed bouncing (points highlighted resulted in $\alpha = 0$ in Figure 4a).

with different B and E will have different β even if they have the same η. A lower value of β will be obtained with lower B and higher E and clear trends can be observed when changing η, while keeping the same B and E. Therefore, when plotting the results of all the blocks together as in Figure 4A, differences are expected. Secondly, MP damping simulations are susceptible to changes in the results with little damping variation, as studied in later sections. Therefore, it is challenging to find a perfect correlation when matching SP damping simulations and dispersion is expected. In those cases where the best matching simulations had $\alpha = 0$ (Figure 4A) the SP damping simulation had low damping, but low values of β still resulted in bouncing not occurring. When attempting to match these SP-damped simulations by instead using MP damping, the required value of α was found to be low which triggered high amplitude bouncing, resulting in further damping of the oscillations. Consequently, the MP damping simulations that most closely matched the SP damping simulations with low β were completely undamped simulations. SP damping simulations took much longer to run and the SP/MP damping ratio of computational times varied from approximately 50 to 350. The eighth block geometry was $\eta = 35°$, which was not included in Figure 4 because upon first contact with the floor during the first oscillation the bounce displaced the block by a large distance and after that the rocking motion ended.

When using MP damping, bouncing of the modelled block after impact was expected (see Section 2.2) and was easily observable from the z displacement of the modelled blocks. An example of block bouncing after impact can be observed in the motion from the block with $B = 0.35$ m, $H = 1.50$ m, and $E = 3600$ MPa (see Figure 5A). The bouncing experienced by all the blocks with MP damping was plotted in Figure 5B to study the relationship between bouncing and block geometry η/R. The bouncing magnitude was measured by the ratio between amplitude and the duration of time that the block remained in the air. Blocks with lower η/R, that is, more slender, exhibited less bouncing, while those with high η/R exhibited greater bouncing as was the case for the block with $B = 0.35$ m and $H = 0.50$ m ($\eta/R \approx 115$ °/m). On the contrary, the simulations with SP damping exhibited no bouncing. No bouncing was reported in the experimental tests included in Section 4, and the bouncing criteria proposed by Lipscombe and Pellegrino[59] suggested that bouncing is only relevant for rather squat blocks of $H/B \leq 3$ if energy damping increases. Therefore, any bouncing in the reported simulations was attributed to high-frequency motions being incorrectly underdamped. From a practical perspective, bouncing was found critical when blocks had approximately $\eta/R > 45$ °/m as seen in the highlighted area in Figure 5B, which corresponds to the simulations that could not be replicated by MP damping due to bouncing (see Figure 4A).

3.2 | Discretised model with zero viscous damping

A commonly used strategy to simulate the behaviour of URM walls is to discretise the model into independent blocks having the same dimensions as the actual masonry units being modelled, connected to each other with cohesive interfaces. Some authors have suggested this approach to be a good strategy to bypass the application of damping by relying on frictional and bond breakage energy dissipation.[21,24]

In Meriggi et al.,[21] top and bottom joints were modelled as perfectly elastic to avoid slippage that was not observed in the experimental tests. The tuff and limestone walls were reported to have $E = 1575$ and 4522 MPa, respectively and joint spacing (l) of 120 and 129 mm on average. If the relationship $k_n = E/l$ is applied as explained in Section 3, as it is used in multiple DEM simulations that were well matched with experimental testing,[28,44,49,60–62] then the joint stiffness

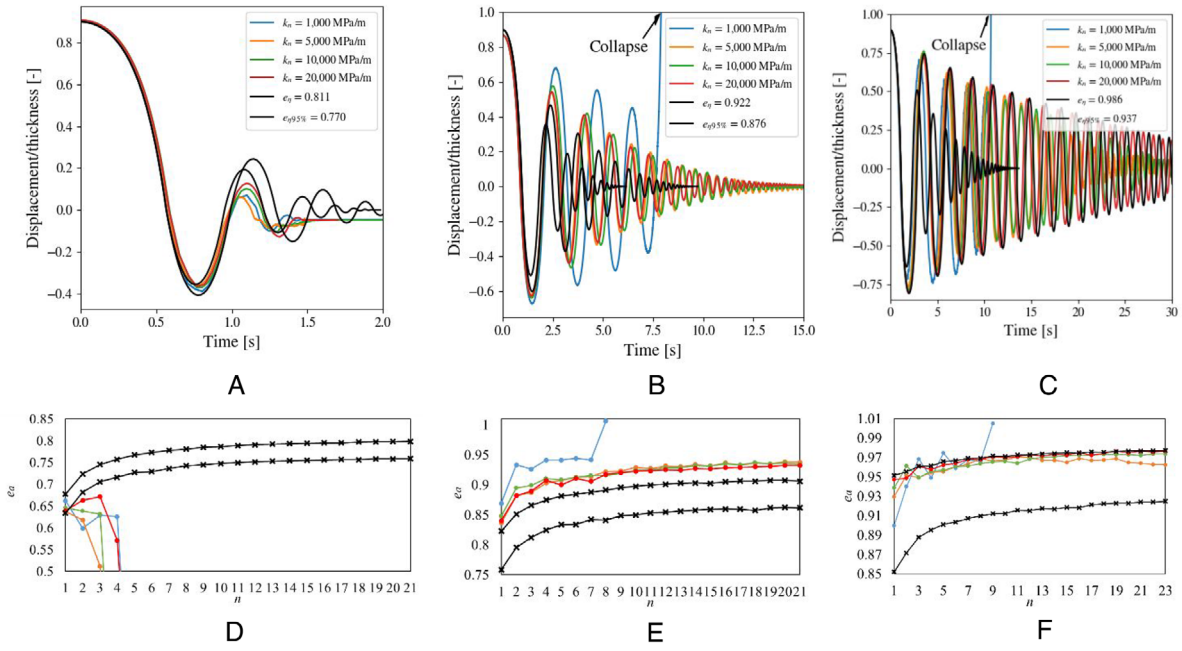

FIGURE 6 Parametric free rocking simulations with varying η. (A) $\eta = 20.8°$ [0.19 m × 0.5 m], (B) $\eta = 13.1°$ [0.35 m × 1.5 m], (C) $\eta = 5.4°$ [0.19 m × 2 m], (D) $\eta = 20.8°$ [0.19 m × 0.5 m], (E) $\eta = 13.1°$ [0.35 m × 1.5 m] and (F) $\eta = 5.4°$ [0.19 m × 2 m].

is 13,125 MPa/m for the tuff wall and 35,084 MPa/m for the limestone wall. However, the joint stiffnesses in Meriggi et al.[21] were tuned to match the experimental fundamental frequency of the walls by performing time-history analyses without damping and by applying a Discrete Fourier Transformation to the results, resulting in $k_n = 490$ MPa/m for tuff masonry and $k_n = 2800$ MPa/m for limestone masonry. Such stiffness values were closer to the stiffness reported by other authors[7,22,26,45] who calibrated their models by best fitting parameters to match experimental dynamic behaviour or by replicating previous similar research. This observed disagreement among different authors could be considered as irrelevant if viscous damping is abandoned, based on the findings of Dimitri et al.[37] who established that joint stiffness had little influence on the dynamic capacity of cohesionless multidrum 2D columns. However, Dimitri et al.[37] did find that when using a friction coefficient of $\mu = 0.46$ a large difference in column dynamic capacity occurred when compared to the results of simulations with $\mu = 0.70$. The column with $\mu = 0.46$ produced simulated sliding between the stone drums that resulted in overturning at higher accelerations than for simulations with $\mu = 0.70$, but only for inputs having a short oscillating period, while longer oscillating period inputs resulted in the multidrum column rocking as a single rigid body. Similarly, varying the MP and SP damping parameters was found to influence the overturning capacity at low input periods and to influence whether the collapse mechanism of the column was sliding or rocking.

The observations described above led to a parametric analysis being performed to better understand the influence of joint stiffness, cohesion, tensile strength and friction coefficient on the rocking behaviour of a cohesive discretised wall without viscous damping applied. Cohesion, tensile strength and friction do not have an influence on the simulation runtime, and therefore a study of simulation runtime was performed with only stiffness variability.

3.2.1 | Stiffness variability

Four different stiffnesses were parametrized in three different block geometries (see Figure 6A–C), with $\gamma = 1800$ kg/m^3 and with joints between bricks having sufficiently high cohesion and tensile strength for no bond connection to fail, in order to solely study the influence of stiffness on damping of the resultant motion. The friction angle, which is relevant for the base joint that opened to allow rocking, was equal to 31°. Widely used rocking models that can be utilised to compute the rocking equation of motion of blocks that are damped by the application of e after each impact were compared to the discretised rocking blocks having no viscous damping applied. Two values of e were used in the comparison: the value based on a geometrical relationship, which is valid for a homogeneous parallelepiped block ($e_\eta = 1 - \frac{3}{2} \cdot \sin^2\eta$), and 95%

TABLE 1 Free rocking apparent damping (e_a) and difference between DEM and simulations using e_η

	$\eta = 20.8°$ [0.19 m × 0.5 m] $e_\eta = 0.811$, $e_{\eta 95\%} = 0.770$			$\eta = 13.1°$ [0.35 m × 1.5 m] $e_\eta = 0.922$, $e_{\eta 95\%} = 0.876$			$\eta = 5.4°$ [0.19 m × 2 m] $e_\eta = 0.986$, $e_{\eta 95\%} = 0.937$		
	Mean e_a	WME (e_η)	WME ($e_{\eta 95\%}$)	Mean e_a	WME (e_η)	WME ($e_{\eta 95\%}$)	Mean e_a	WME (e_η)	WME ($e_{\eta 95\%}$)
k_n = 1,000 MPa/m	0.629	0.846	0.841	0.938	0.657	0.684	0.959	0.618	0.644
k_n = 5,000 MPa/m	0.589	0.892	0.886	0.918	0.031	0.091	0.963	0.008	0.058
k_n = 10,000 MPa/m	0.639	0.883	0.878	0.919	0.032	0.092	0.966	0.006	0.062
k_n = 20,000 MPa/m	0.636	0.844	0.836	0.915	0.027	0.086	0.969	0.002	0.065

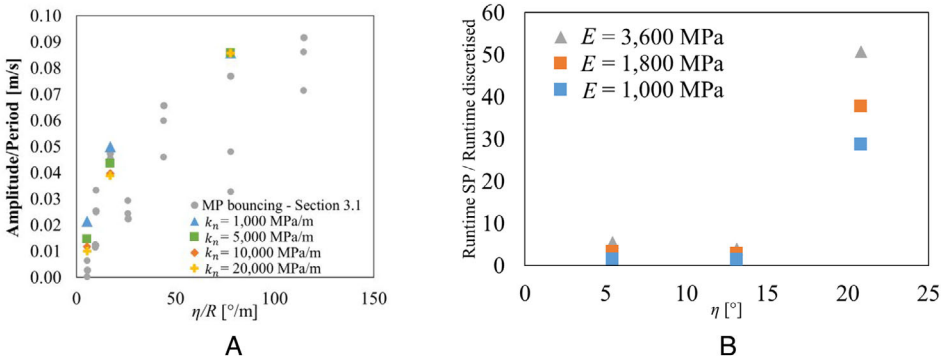

FIGURE 7 Result analysis of the parametric simulations. (A) Relationship between block dimensions and observed bouncing and (B) Ratio between SP damping runtimes and discretised model runtimes.

of e_η ($e_{\eta 95\%}$) as suggested by Sorrentino et al.[63] as a closer value to experimental observations. To process the differences between time-histories the apparent coefficient of restitution (e_a), shown in Equation 6[63,64] was computed and is shown in Figure 6D–F. In Equation 6, $|\theta_n|$ is the maximum absolute rotation at the n^{th} bounce. The e_a represents the energy that was dissipated after each impact between the block and the ground, with a larger value of the coefficient of restitution representing less energy dissipation. The damping that resulted from each simulation was studied by comparing the trends in Figure 6D–F and analysing the WME in Table 1 for e_a at each impact compared to that of the simulation using e_η and $e_{\eta 95\%}$ as input parameters. Sorrentino et al.[63] found that e_a is less than the calculated value e_η and that the first few impacts generally have a lower e_a than the subsequent series of values. The same trends as noted by Sorrentino et al.[63] are evident in Figure 6E–G.

$$e_a = \sqrt[2n]{\frac{1-\left(1-\frac{|\theta_n|}{\eta}\right)^2}{1-\left(1-\frac{|\theta_0|}{\eta}\right)^2}} \tag{6}$$

In certain cases, low stiffness caused overturning midway through the decaying damped motion that is phenomenologically incorrect (see Figure 6B,C,E,F). The bouncing magnitude of the blocks was similar to values that were obtained for the MP damping simulations reported in Section 3.1, although higher k_n values caused reduced bouncing (see Figure 7A). The large bouncing observed in the block with $\eta = 20.8°$, regardless of the value of k_n, caused rapidly-decaying energy dissipation in the time-history simulation as seen in Figure 6A,D and Table 1. No trend was clearly observable from Figure 6 and Table 1 that systematically correlated the change in k_n and the level of damped motion except for simulations with $\eta = 5.4°$ that showed an ascending trend of energy dissipation with lowering k_n. With the exception of simulations in which a very low stiffness was implemented, simulations using different k_n with $\eta = 5.4°$ and $\eta = 13.1°$ showed almost no difference in energy dissipation (see mean values of e_a in Table 1). Overall, the results of DEM simulations with $\eta = 5.4°$ and $\eta = 13.1°$ were closer to the results for e_η than those results for 95% of e_η (see values of WME in Table 1), leading to an underestimation of damping in the DEM simulations when compared to most physical experiments represented by 95% of e_η, as demonstrated by Sorrentino et al.[63] However, the SP damping simulations reported in Section 3.1 and undertaken by

applying damping at the frequencies discussed in Section 2.2 showed a more highly damped response, being closer to 95% of e_η, without bouncing or rotation effects. For the exclusive purpose of runtime comparison, new SP damping simulations were developed to match the discretised simulations. The runtimes of the discretised models were from approximately two to five times more efficient than for the SP damping simulations, except for the geometry $\eta = 20.8°$ where the runtimes were from 30 to 50 times more efficient (see Figure 7B).

3.2.2 | Cohesion, tensile strength and friction variability

Based on the findings of the stiffness parametrization study reported in the previous section, the block with $\eta = 5.4°$ and $k_n = 10{,}000$ MPa/m was selected to investigate the role of cohesion (c), tensile strength (f_t), and friction coefficient (μ), due to the very low bouncing observed (see Figure 7A), thereby avoiding any influence in the damped motion that was potentially related to bouncing. The block with $k_n = 20{,}000$ MPa/m was discarded because such a high stiffness made for long computational time. The cohesion and tensile strength of the joints were parametrised as 0.1 and 0.5 MPa and 0.1, 0.3, 0.5 MPa, respectively, including values as low as 0.1 MPa to allow for joint breakage and to observe the influence of cracking of the discretised model during the rocking motion. Similarly, the friction coefficient was parametrised as 0.30, 0.50, and 0.75 including low values that could be found in real URM structures and would allow the role of interface sliding in the rocking behaviour to be observed.

Joints fail either in shear, which is controlled by c and μ, or fail in tension, which is governed by f_t, with both failure modes causing damped motion due to energy dissipation. After the sub-contacts in the joints failed in either tension or shear only frictional interaction was observed, making it difficult to assess the cause of the damped motion of the model by only observing the failure type. Hence, to parametrically study the damped motion of the model the parameters μ and f_t were paired with very high and very low values of c (see Figure 8) that conditioned the development or non-development of shear failure. The free rocking time-histories and e_a for the combination of c and μ were plotted as shown in Figure 8A,C, and for the combination of c and f_t were plotted as shown in Figure 8B,D. The trends of the e_a plots obtained for each simulation resulted in a steeper slope when the bond strength parameters were weak and resulted in a shallower slope when strong bond was applied (Figure 8C,D), agreeing with the trend observed in Section 3.2.1 (see Figure 6F) of shallower slopes when the bonds were modelled as being strong enough to cause a low level of damage. As seen in Figure 8C,D, the values of e_a fluctuated at different points of the simulations, meaning that after the fluctuation points that alter the trend slope, failure in the joints occurred changing the energy dissipated in each impact. For the first few impacts before failure a high value of cohesion was found to correlate with low energy dissipation (see Figure 8C,D) and f_t was highly influential only when no major shear failure occurred (difference between $c = 0.5$ MPa, $f_t = 0.1$ MPa and $c = 0.5$ MPa, $f_t = 0.3$ MPa), while the influence of μ was found to be less pronounced. In all simulations the shear or tensile failure of joints was clearly visible, except for the combination $c = 0.5$ MPa, $f_t = 0.5$ MPa, and $\mu = 0.7$. One of the main drawbacks of using discretised models that rely on damage for damped motion is that in the experimental results, no damage was observed in the block other than at the base joint.

3.3 | Dependency of rocking motion on interface integration points

An important factor that contributes to the level of damped motion of rocking blocks and to the computation time of the simulation is the division of the contact interface between the block and the foundation. It is well known that when the contact interface is more refined, the obtained solution will have a smoother transition from the elastic phase to the rocking phase, whereas if the interface is not refined enough the result will be closer to a rigid interface case. In DEM, each contact point between blocks defines an integration point to compute the stress distribution within the contact surface (see Figure 3A). Specifically for 2D quasistatic DEM simulations, Pulatsu et al.[65] calibrated elastic blocks using parametric analysis and observed when the results of successive simulations with an increasing number of contact points achieved similar responses. However, because an increased number of contact points increases the computational time, six contact points between elements was observed to be a suitable number of thickness integration points. Similarly, Shawa et al.[58] fitted their model by comparing a pushover curve with a Winkler-type foundation, considering 16 sub-contacts as being most appropriate. Godio et al.[66] researched the interaction problem for rigid elements and offered recommendations for one-way bending walls in 3D based on a relationship between horizontal and vertical reaction forces. It was also found that a reasonable balance between computation time and accuracy was obtained when using nine sub-contacts, which

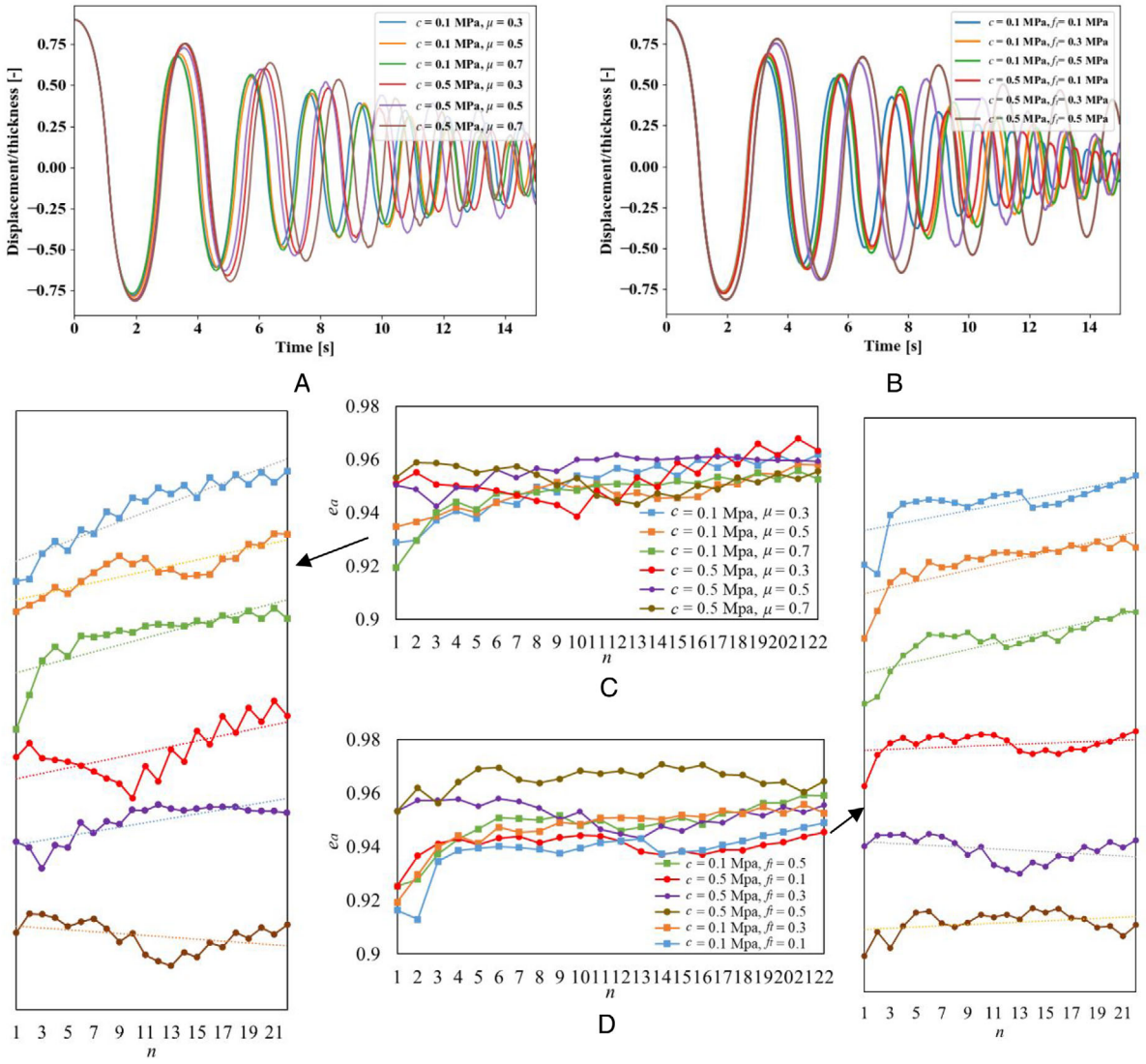

FIGURE 8 Free rocking time-histories and apparent damping (e_a) for blocks with $\eta = 5.4\,°$ and $k_n = 10{,}000$ MPa/m. (A) $f_t = 0.3$ MPa, (B) $\mu = 0.7$, (C) $f_t = 0.3$ MPa (independent plots on the left including general trend) and (D) $\mu = 0.7$ (independent plots on the right including general trend).

was later applied by Godio and Beyer[28] in 2D dynamic simulations. For 3D simulations, Lemos[67] and Lemos[68] explored the types of contacts and the discretization possibilities in terms of triangular or rectangular faces and levels of discretization for rigid and deformable blocks in order to correctly compute the eigenvalues of a stepped cantilever wall and a square column, recommending at least three contact points across the thickness. Most researchers investigating 3D rocking blocks have used DEM to simulate the response of multi-drum pseudo-cylindrical columns, which have been approximated using a polygonal cross-section where the geometry of every drum naturally creates several contact points for a correct computation of the stress distribution.

Based on a study performed by Shawa et al.[58] for 2D DEM, blocks with different numbers of interface integration points and with $B = 0.2$ m, $H = 2$ m, depth $(L) = 1$ m, a very large friction coefficient to prevent sliding ($\mu > 5$), density $(\gamma) = 1800$ kg/m^3 and $E = 1800$ MPa were modelled herein to simulate a pushover analysis and compare their capacity curves (see Figure 9A). The difference in the dynamic performance between blocks with different numbers of integration points was also investigated using SP damping ($\beta = 0.00693$, according to Sections 2.2 and 3), to avoid any rattling or bouncing (Figure 9B) and the computational time of each simulation was recorded (see Table 2, CPU Intel Xeon E5-2698 v3 @2×2.30 GHz, 36 GB RAM). The blocks with 10 and 15 integration points were observed to provide a smooth, accurate prediction of the real quasistatic behaviour of a rocking URM wall, while blocks with two and five contact points showed higher resistance to initiate rotation, resulting in a predicted response that was closer to the ideal rigid block and

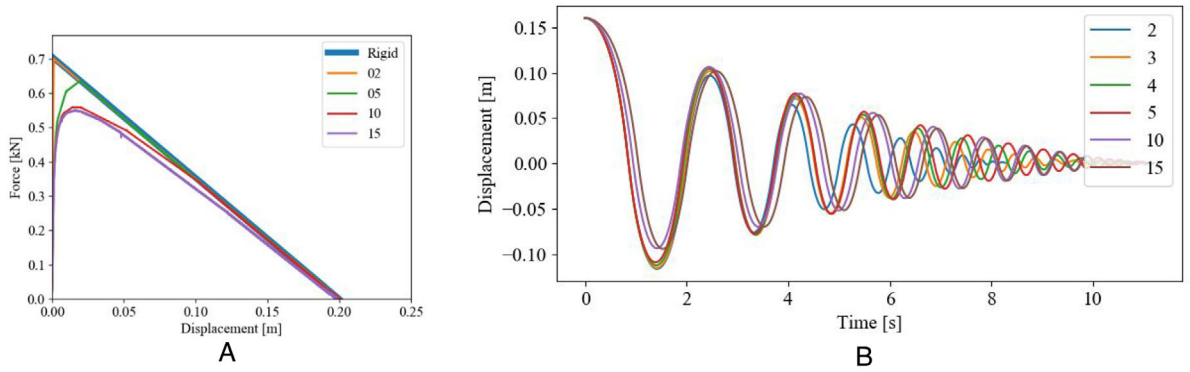

FIGURE 9 Block response for different numbers of interface integration points. (A) Pushover curves and (B) Free rocking histories.

TABLE 2 Change in computational time with interface contact points for the free rocking analyses

Contact points	2	3	4	5	10	15
Computation time (h)	6	13	16	20	34	54

rigid foundation bi-linear behaviour. In Figure 9B more damped oscillations can be observed when fewer contact points were implemented. This difference in damped behaviour is a consequence of the decrease in the spring stiffness with increasing number of contact points (Equation 2) and therefore the rocking amplitude of the block increased with more contact points (see Figure 9B). Similar performance of the block was obtained when 10 and 15 contact points were implemented. However, a significant change in computational time was observed when adding contact points as can be seen in Table 2.

4 | ARTIFICIAL SUPPORT FOR DAMPING STRATEGY SELECTION BASED ON DECEPTIVE MATCHING OF RESULTS

Following the study of possible sources of inaccuracy, various laboratory tests of free rocking and earthquake-induced rocking parapets, façades and one-way bending walls were simulated using MP and SP damping. The MP and SP damping parameters α and β were adjusted to match the free rocking experiments, and later, the same values were used to simulate the same rocking element subjected to earthquake motion. The values of α and β used in the parapet and façade experiments were plotted against the values obtained in Figure 4A to observe how close the simulations were to the previously obtained relationship. Discretised models were also included in the experimental simulations whenever possible.

4.1 | Rocking parapets

The first experiment that was simulated was the free rocking test performed by Giaretton et al.[69] of an URM parapet. Four models were compared against the experimental test using the mechanical properties provided in Giaretton et al.[69]: two models with the geometry discretised into multiple blocks (no damping applied), a third as a single block (Figure 10C) with MP damping, and a fourth having the same discretised geometry and SP damping. At the contact interface with the foundation a total of 7 mm was removed from the 230-mm thickness reported by Giaretton et al.[69] to take into consideration crushing of the very soft mortar after the rocking motion commenced. The material properties implemented in the discretised model were extracted from Giaretton et al.[69] as $c = 0.5$ MPa, $f_t = 0.1$ MPa, and $\mu = 0.60$, while $\gamma = 1800$ kg/m^3 and $E = 1800$ MPa were assumed for all the models. These tensile strength and cohesion parameters caused extensive damage in the joints of the discretised model (35% of sub-contacts in the model exhibited shear failure and 55% of the sub-contacts in the model exhibited tensile failure), which resulted in extensive damping of the rocking motion (see Figure 10B). Applying the lessons learnt in Section 3.2.2, c and f_t were increased until a reasonable match with the experiment was obtained, reaching $c = 0.6$ MPa and $f_t = 0.5$ MPa (18% of the sub-contacts in the model exhibited shear failure and 19%

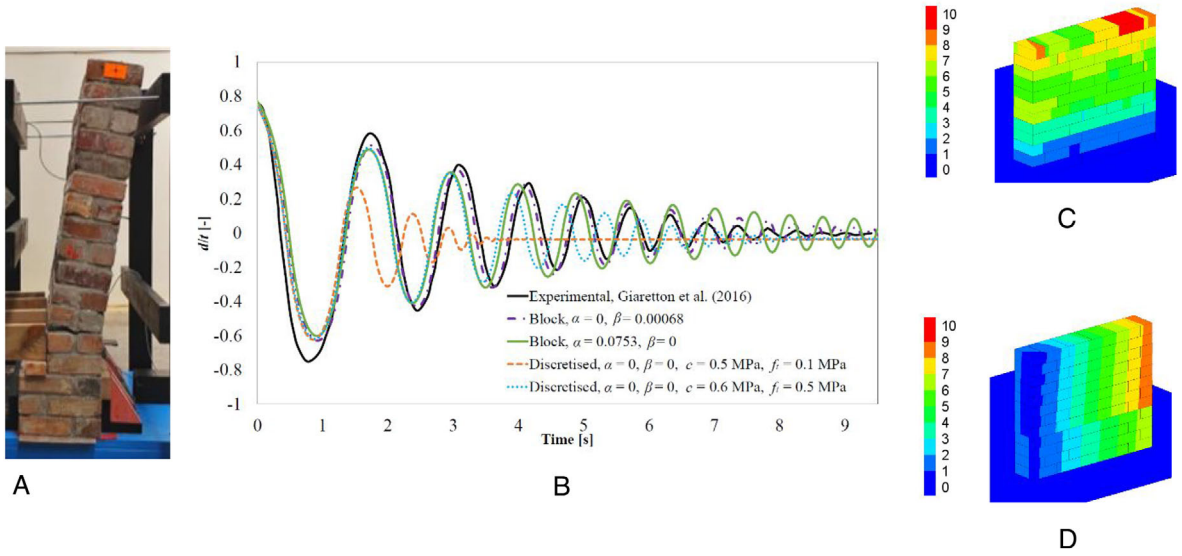

FIGURE 10 Free rocking motion of URM parapet. (A) Experimental setup[69], (B) Non-dimensional top displacement vs time, (C) Discretised parapet drift [mm] at the end of the simulation, with $c = 0.5$ MPa and $f_t = 0.1$ MPa and (D) Discretised parapet drift [mm] at the end of the simulation, with $c = 0.6$ MPa and $f_t = 0.5$ MPa.

of the sub-contacts in the model exhibited tensile failure). While the motion of the lower-strength discretised model was damped due to a distributed failure of the joints, with some blocks completely detaching from the wall (see Figure 10C), the higher-strength discretised model had a main horizontal crack and torsion (due to the non-symmetrical masonry bond pattern and the multiple possibilities of joints failure propagation) was observed in the remaining top and bottom pieces (see Figure 10D). Numerical results indicated that good agreement with the experimental displacements could be reached with every modelling strategy (Figure 10B), despite the motion being underdamped for high frequencies using MP damping. The single block models that best fit the experimental free rocking using SP and MP damping had $\alpha = 0.0753$ and $\beta = 0.00068$, respectively, with the SP damping simulation being the best matching of all the alternatives. However, when applying the formulation given in Sections 2.2 and 3 ($\beta = 0.00305$) the motion was overdamped as seen in Figure 10B, indicating that the formulation explained needs further improvement.

Part of the Giaretton et al.[69] testing campaign consisted of subjecting a set of parapets to earthquake motions with an increasing intensity measure until reaching overturning. A simulation was also performed for the last test of the increasing test series on a partially cracked parapet that was undamaged at the beginning of the experiment. The parapet tested by Giaretton et al.[69] still had cohesive resistance at the beginning of the simulated test, which added uncertainty to the simulation strategy and required extra parametrical work to accurately introduce the tensile strength. Due to the large drift error observed on the discretised free rocking model, only the single block model was simulated for the earthquake time-history.

Different values of tensile strength applied at the base interface triggered the start of the rocking motion at different times of the earthquake, completely changing the history of the motion. Therefore, accurately obtaining the tensile strength at the base was crucial. While in Giaretton et al.[69] the tensile strength of the mortar samples was given as 0.07 MPa, the optimal tensile strength for matching of the simulation was 0.10 MPa in the MP damping simulation and 0.06 MPa in the SP damping simulation, showing the tendency of the MP damping simulation to collapse at an early stage. The rest of the parameters of all models remained the same as given by Giaretton et al.[69] Values of $\alpha = 0.0753$ and higher were not enough to prevent the premature collapse of the parapet using MP damping (Figure 11A). Conversely, SP damping provided a consistent prediction of the parapet response and collapse while varying $\beta = 0.00068$ (see Figure 11B).

4.2 | Rocking façades

Most of the studies performed on rocking blocks were focused on freestanding parapets or one-way bending walls. However, observations after earthquakes have shown that most macroblocks cannot complete a full oscillation because of

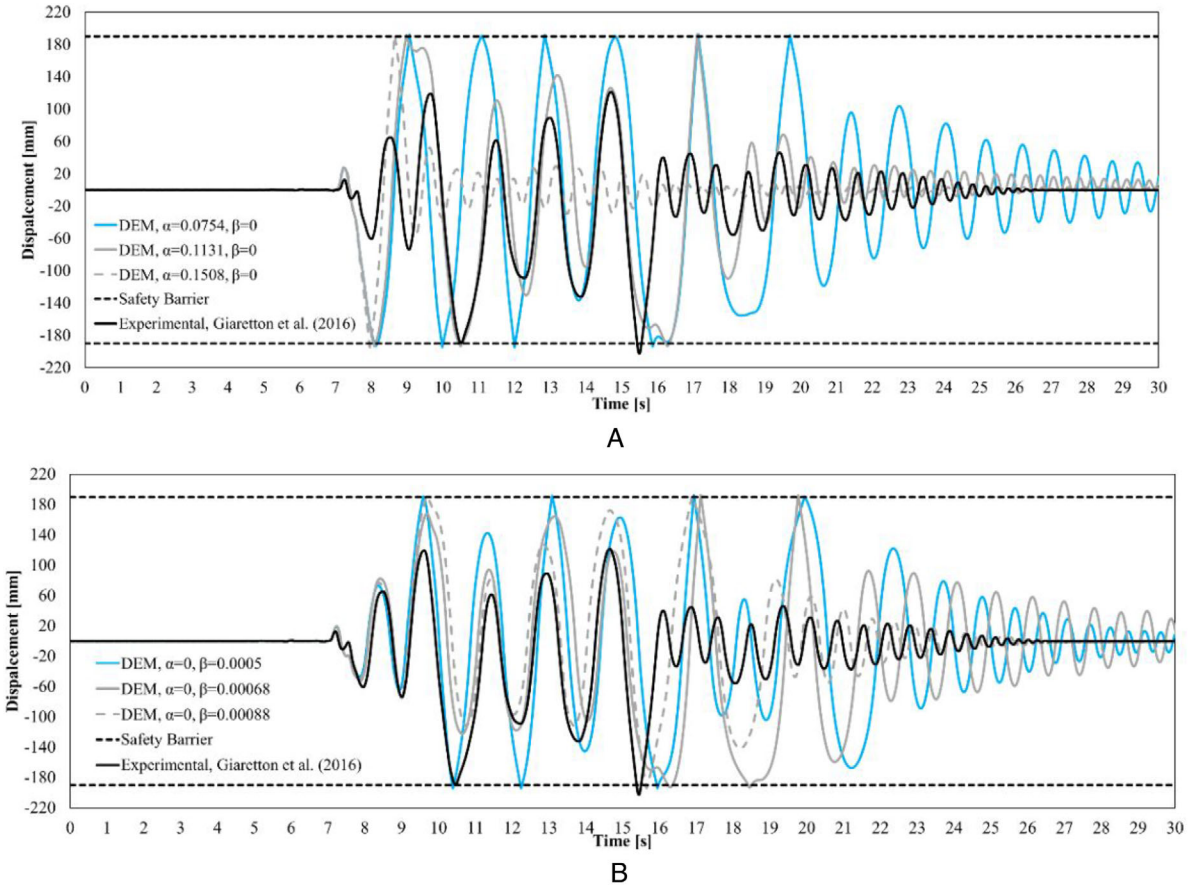

FIGURE 11 Free rocking top displacement of URM parapet. (A) MP damping and (B) SP damping.

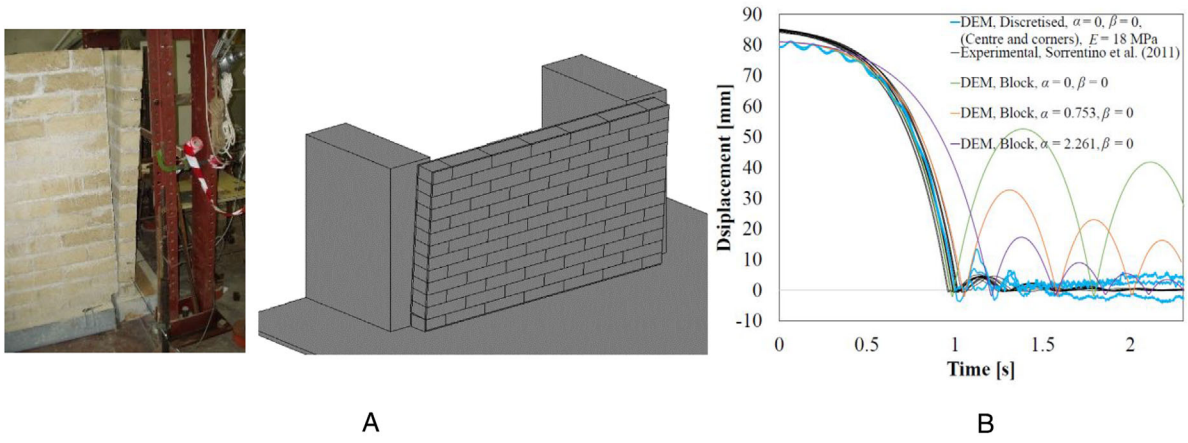

FIGURE 12 One-sided free rocking: comparison between experimental and numerical discretised and single-block models. $\mu = 0.60$, $\gamma = 1750$ kg/m^3, and $E = 1800$ MPa, unless otherwise noted. (A) Experimental setup[63] and DEM discretised model and (B) Displacement vs time.

contact with transversal structures, referred to as one-sided rocking or 1SR. The experimental setup reported by Sorrentino et al.[63] was used to test the limits of using MP damping for 1SR because the block had to impact the ground and the return walls (Figure 12A), resulting in a greater likelihood of the impact frequencies being underdamped and introducing inaccuracies into the simulation.

As observed in Figure 12C, low levels of damping were insufficient to damp the motion of the 1SR wall when a solid block was used to simulate the façade. High levels of damping not only affected the amplitude of the rebound but also the

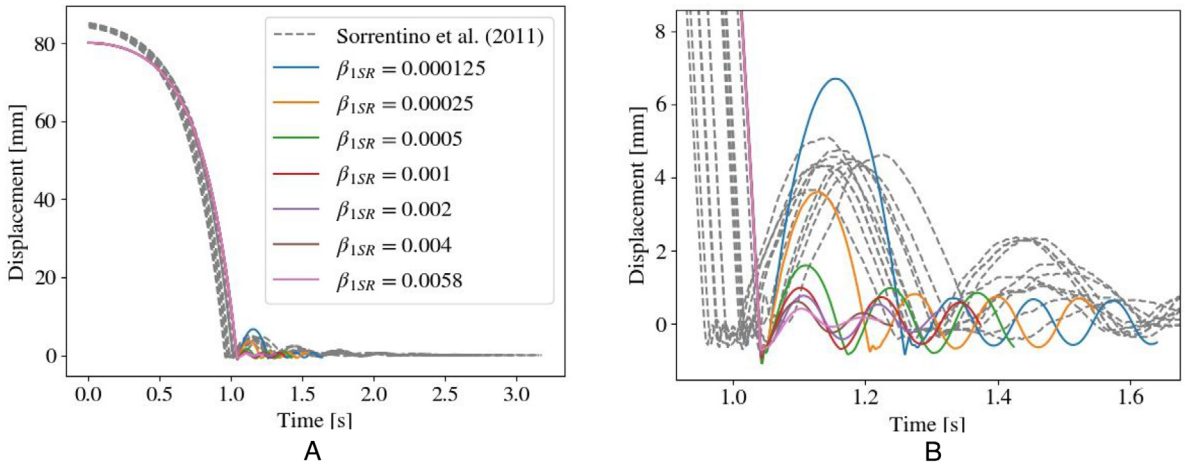

FIGURE 13 DEM simulations and experimental testing from Sorrentino et al.[63] (A) Complete time-history and (B) Zoom in between 0.9 and 1.7 s.

period of the first quarter cycle of the free rocking because MP damping overdamped the low-frequency motion. Therefore, the model using a single block was considered to not be the best option to simulate 1SR. A secondary option that involved discretising the wall into as many blocks as bricks in the real specimen (see Figure 12A) and not applying any viscous damping was modelled. When $E = 1800$ MPa was used, not shown for the sake of clarity, very similar behaviour was obtained as for the single block strategy with no damping. Lowering c and f_t resulted in only a minor difference to the dynamic behaviour until the strength was low enough to impose permanent strong deformation to the wall. Only when E was reduced by a factor of 10^{-2} did the simulated behaviour become closer to the experimental results, but with strong rattling effects also observed (see Figure 12B). Residual drift was observed at the top of the wall due to a combination of the rattling effect and damage of the joints, resulting in a 4 mm rotational displacement at the top of the wall as seen in the plot of the three points at the top (corners and centre, see Figure 12B).

The abovementioned experimental setup developed by Sorrentino et al.[63] was also simulated using SP damping, including the reported imperfections of rounded edges in contact with the base. One-sided rocking, where the block experiences a double impact with the foundation and one impact with the return wall, was not covered in DeJong[43] and when applying the single block strategy described in Section 2.2, the results did not replicate the experiments. As commented in Section 3, the ω_{crit} of the wall impacting the return walls is significantly higher than that of the single rocking block impacting the foundation. The β value, for a wall having $B = 0.11$ m, $H = 0.8$ m, $L = 1.5$ m, $\mu = 0.60$, $\gamma = 1750$ kg/m^3 and $E = 1800$ MPa obtained using the formulation from Section 2 was 0.00017 for the 1SR model and 0.00470 for the two-sided rocking block. As seen in Figure 13, the best fitting simulation occurred for $\beta = 0.00025$, although the rocking motion after the majority of the energy was dissipated remained undamped without causing rattling. The same phenomena occurred for simulations with $\beta = 0.000125$, 0.000500, and 0.001000. In contrast, simulations with $\beta = 0.00200$, 0.00400, and 0.00580 were found to be overdamped after the first impact. It is worth noting that, even when accounting for the drawback of the undamped motion at the end of the free rocking, SP damping provides a significantly better simulation than that obtained using MP damping (see Figures 12B vs. 13).

Simulations using MP damping were not capable of realistically simulating 1SR free-rocking tests. However, in order to observe the consistency and approximation of the MP damping model to simulate 1SR blocks subjected to earthquakes, the experimental campaign reported by Shawa et al.[58] was simulated. It is worth noting that Shawa et al.[58] reproduced the 1SR tests with both an analytical model based on the Housner[64] approach taking into account the appropriate coefficient of restitution for energy dissipation due to multiple impacts, and with a 2D DEM model using SP damping. By means of a lengthy and tedious trial and error procedure, values for α were obtained that enabled a close approximation to 1SR walls subjected to four earthquakes named BagnirWE, SturWE, R1168EW, and CalitWE (more information can be found in Shawa et al.[58]). A physical gap of 4 mm was left between the return walls and the overturning wall as specified in Shawa et al.[58] A slope under the wall was observed in the experimental campaign, caused by dust and crushed material accumulation. The magnitude of this slope increased test after test and had to be simulated by adding the slope with an angle φ. Rounded corners with 8 mm radius at the bottom of the wall were also included to simulate crushing and wearing due to the rocking motion. An acceptable agreement was obtained, as observed in Figure 14 where the damping that best

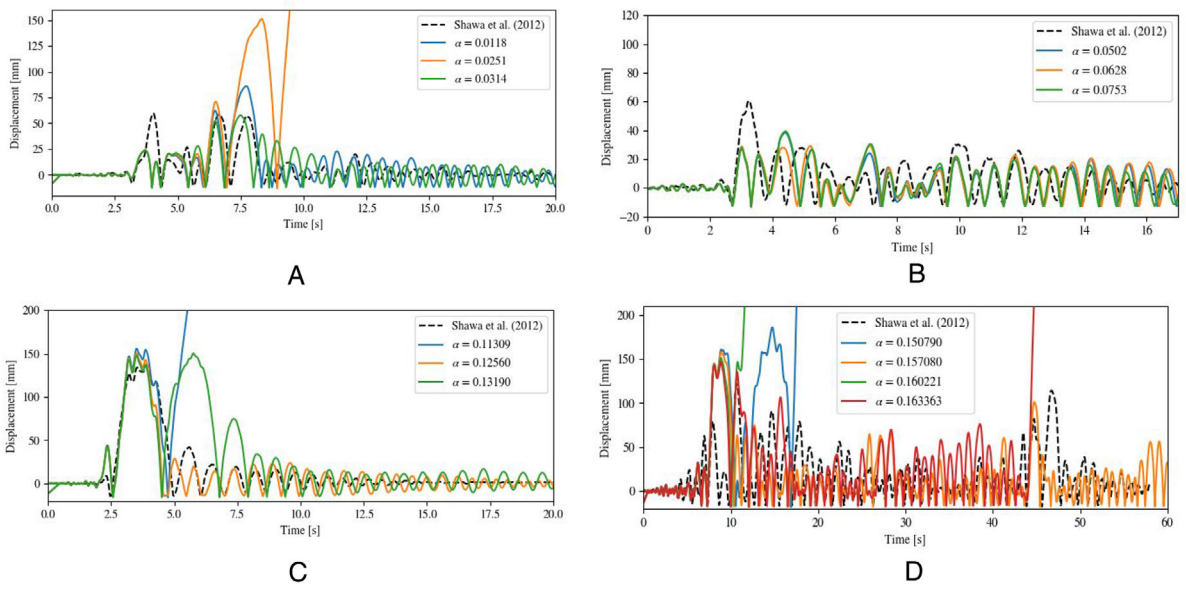

FIGURE 14 Comparison of top displacement between experiments and DEM simulation. (A) BagnirWE, $\varphi = 0.191°$, (B) SturWE, $\varphi = 0.210°$, (C) R1168EW, $\varphi = 0.272°$ and (D) CalitWE, $\varphi = 0.348°$.

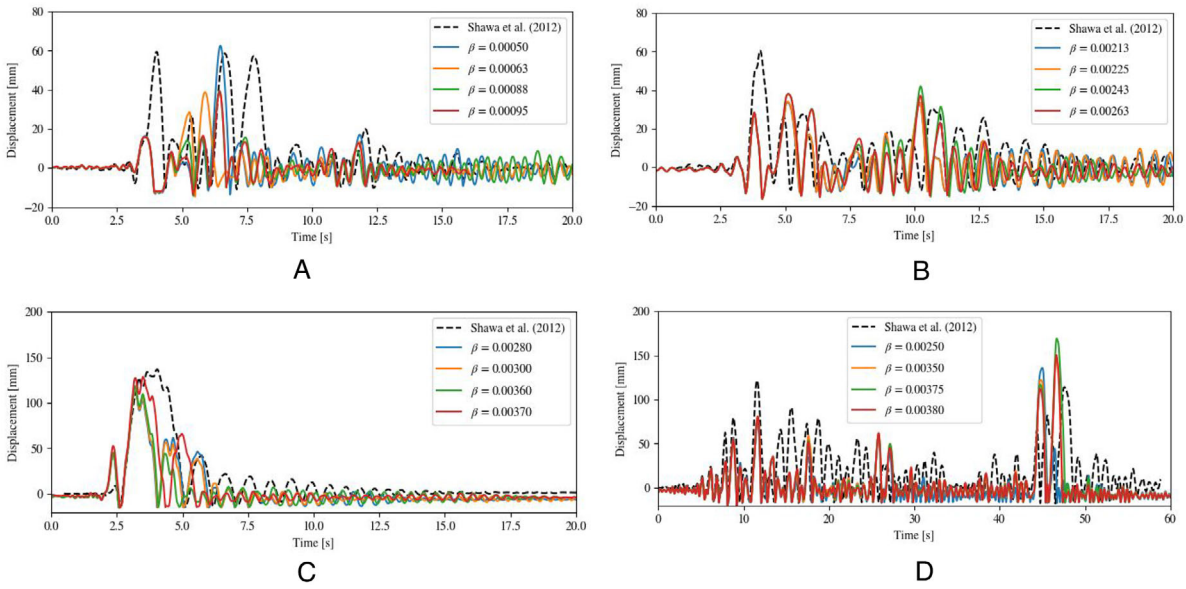

FIGURE 15 Comparison of top displacement between experiments and DEM simulation. (A) BagnirWE, $\varphi = 0.191°$, (B) SturWE, $\varphi = 0.210°$, (C) R1168EW, $\varphi = 0.272°$ and (D) CalitWE, $\varphi = 0.348°$.

fitted the solution is plotted together with minimal variations of α. Small changes in α changed the history of the motion, showing significant differences in displacements (see Figure 14A,C,D) as opposed to the SP damping approach used in Shawa et al.[58]

Similarly, to the free rocking blocks, the 1SR walls tested by Shawa et al.[58] were simulated using SP damping. Considering $\beta = 0.00025$ as the value obtained in the free rocking tests for a non-deteriorated wall, β was gradually increased for the testing sequence described in Shawa et al.[58] Good agreement was found between experimental observations and 3D DEM with SP damping simulations (see Figure 15). Little difference in the rocking performance between simulations with varying β values was observed (see Figure 15), with results being robust for explored variations of damping coefficient. The results obtained by Shawa et al.[58] using UDEC (2D DEM software developed by Itasca[11]) were similar to the ones obtained herein, but not identical due to current simulations having an extra dimension that allows for different boundary

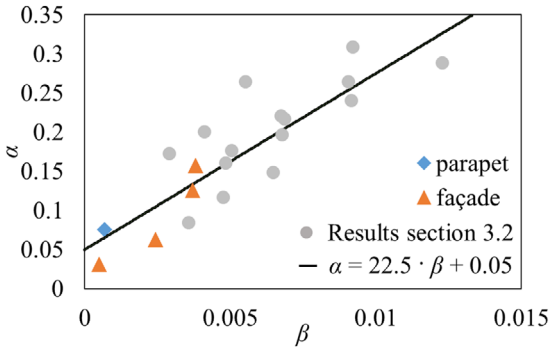

FIGURE 16 Pragmatic linear relationship between α and β derived from best matching α and β values for Shawa et al.[58] façades and for Giaretton et al.[69] parapets. Parapet results from the parametric analysis reported in Section 3.1 were also included

conditions, rotation about the vertical axis, and the use of different amounts of interface integration points. The result of these differences at an early stage of the simulations influences the complete time-history.

4.3 | Using MP damping to approximate correct use of SP damping

The damping values of α and β for those simulations that best matched with the experimental tests described in Figures 10, 11, 14, and 15 were plotted in Figure 16. These best-matched values of α and β were observed to follow the same trend as the results reported in Figure 4A (included in Figure 16) from matching MP to SP damping simulations following the DeJong[43] method (see Section 2.2) to assign β, without including the simulations that were strongly influenced by undamped bouncing. A linear best fit regression of the combined data was undertaken and a pragmatic relationship was developed as $\alpha = 22.4 \cdot \beta + 0.05$ (see Figure 16). The exercise of matching the MP-damped DEM simulations to the experimental tests needs to be interpreted carefully because, as observed in the simulated parapet and façades subjected to earthquake motion (Figures 11A and 14), small input changes can lead to bouncing and incorrect rocking and overturning. Nonetheless, the trend observable from the point cloud shown in Figure 16 offers an approximation of α from β that can be estimated from material and geometrical properties of the block as explained in Sections 2.2 and 3. This relationship offers a tool for a first approximation of the results using MP damping, that should later be refined using SP damping simulations.

4.4 | Vertically spanning rocking walls

After simulating single-block URM parapets and façades, a one-way bending wall composed by two blocks rocking on top of each other was modelled to explore the relationship between MP and SP damping. For this purpose, a set of laboratory tests performed by Griffith et al.[70] with $B = 0.11$ m, $H = 1.50$ m, $L = 0.95$ m, were simulated using $\mu = 0.70$, $\gamma = 1800$ kg/m^3. The value of Young's modulus was not stated by Griffith et al.,[70] so the rather low value of $E = 48$ MPa as obtained by Godio and Beyer[28,71] within an Euler beam framework by matching experimental and analytical capacity curves was used herein. In such tests Griffith et al.[70] recorded the displacement d at the mid-height of pre-cracked walls left to freely rock from an initial displacement. One of the most challenging details to model from the experimental campaign was the boundary conditions (see Figure 17B,C). Theoretically designed as a vertically rolling support, the top connection needed to allow vertical sliding of the wall with minimum resistance while at the same time restraining the horizontal displacement. Additionally, the connection needed to be independent from the wall and capable of transmitting motion if earthquake input was to be modelled. Consequently, rod elements with zero friction were modelled at the same height as in Griffith et al.[70] to emulate the real setup (see Figure 17B). As seen in Figure 17C, a secondary moving rod was modelled to push the centre of the wall to its initial rocking position.

The value of $\alpha = 0.7539$ was chosen when reaching the minimum weighted mean error between both displacement time-history results (same procedure as in Shawa et al.,[58] see Figure 17A). For the SP damping simulation, β was obtained as 0.0032 using the formulation explained in Sections 2.2 and 3, which is a very similar value to that obtained by Godio

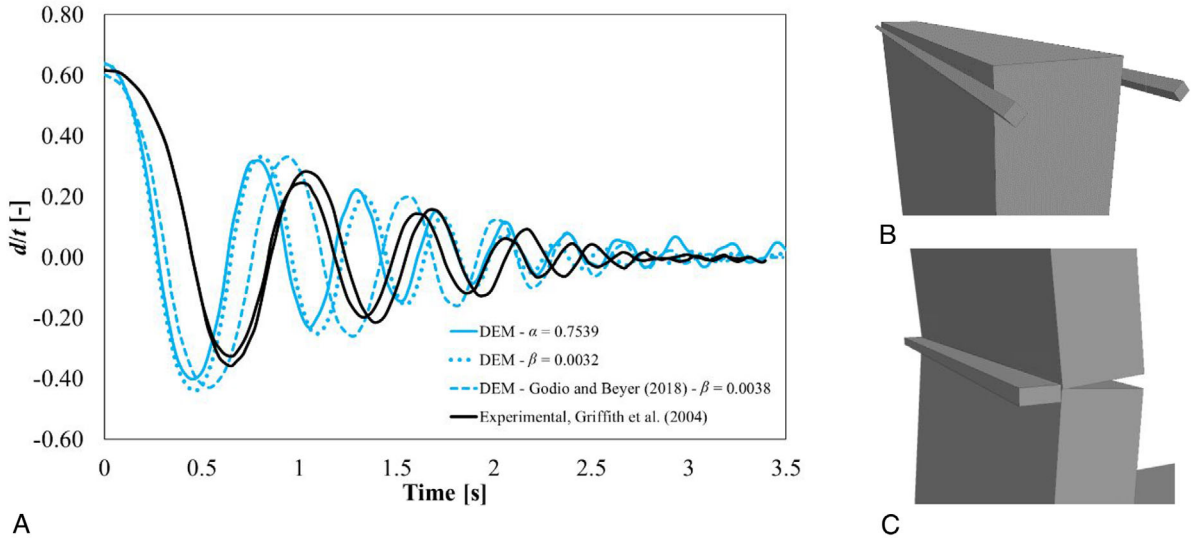

FIGURE 17 Free rocking motion of one-way bending wall. (A) Time vs non-dimensional mid-height displacement, (B) Top boundary condition and (C) Mid-height crack.

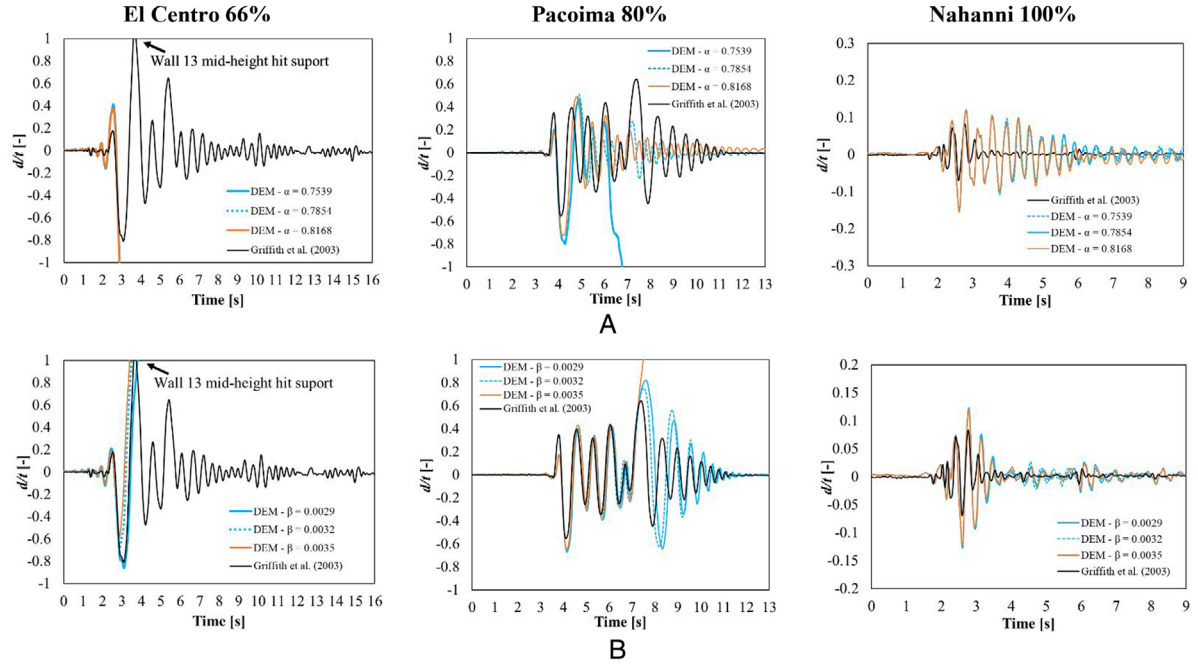

FIGURE 18 Rocking motion of one-way bending walls subjected to earthquakes. (A) MP damping and (B) SP damping.

and Beyer[28] ($\beta = 0.0038$). In addition to modelling free rocking oscillations, the same one-way bending walls tested by Griffith et al.[70] when subjected to three different earthquakes were simulated as well. Three earthquake ground motions with different amplitude scaling factors were considered, being El Centro earthquake at 66% of the original accelerations, Pacoima at 80% and Nahanni at 100%. The simulations showed very good agreement with the tests when the same β was applied as for the free rocking test (see Figure 18A). Simulations using MP damping (see Figure 18B) predicted an approximated motion of the wall, although not as good as the SP damping simulations. As outlined by Griffith et al.,[70] vibration frequency and damping ratio could be related to overburden of the walls. A parametric study of vertically spanning rocking walls including viscous damping, with different overburden loads and subjected to different earthquakes was studied by Godio and Beyer.[28]

5 | CONCLUDING REMARKS

Rocking motion is frequently associated with the response of URM structures when subjected to earthquake excitation and a type of behaviour that can be effectively modelled using the DEM. The damping phenomena present in rocking motion and the frequencies associated with this motion were investigated herein. The energy dissipation strategies necessary to damp these frequencies were presented, together with an investigation of the effect that several parameters have in damping the rattling effect and damping of the frequencies associated with rocking impacts.

Discretised rocking block models with varying geometries were studied by parametrising joint material properties without applying Rayleigh damping, based on the suggestions of previous authors regarding a methodology for how to bypass the application of damping by instead relying on energy dissipation due to friction and bond (cohesion) breakage. Due to the energy released when either shear or tensile cracking occurs, the apparent damping associated with friction and bond was found to be heavily dependent on the adopted values of cohesion and tensile strength, but it was found that tensile strength was only influential when no major shear failure occurred. Low values of cohesion and tensile strength led to damage due to crack opening and block sliding and associated damped motion, whereas the friction coefficient was found to be less influential in generating damped motion. Varying the joint stiffness was found to have less influence on rocking motion when compared to the effect of varying either cohesion or tensile strength, and it was identified that low magnitudes of joint stiffness (1000 MPa/m) caused non-realistic results and false forecasts of overturning. Squat blocks (with high η) experienced significant bouncing that hid the effect of varying the joint stiffness and that reduced the influence of cracking and frictional dissipation of the joints. Bouncing due to non-damped high frequency motion in the discretised models was the same as when MP damping was used, and the runtime was 30–50 times faster than when applying the SP damping approach. As a consequence of bond cracking, discretised models that were developed to simulate parapet testing resulted in residual drift that did not occur in the experiment, and the overall motion replicated the experimentally-observed motion only when joint strength values were purposely adapted to match the experimental data. The discretised strategy was implemented for façades, but the experimental displacement response could not be replicated without generating either extensive damage that was not observed experimentally, a strong rattling effect or an insufficiently damped motion, regardless of the joint parameters used.

The conclusions regarding discretised models discussed herein are focused on cohesive rocking masonry parts, which are different from dry-stacked masonry, but can be extrapolated to complete discretised masonry buildings. Based on observation from the reported study, for complete masonry buildings where collapse or near collapse is expected, the introduction of SP damping is recommended in order to control rattling and allow rocking without bouncing, and cohesive joints stronger than 0.1 MPa are recommended in order to avoid excessive damped motion due to joint damage.

Sufficient matching of simulations with MP damping against experimental results was only possible for free rocking parapets and one-way bending walls. However, these simulations required trial-and-error calibration of a known result because small changes of α resulted in significant discrepancies. Parapets subjected to earthquake motion and one-sided rocking blocks that simulate rocking URM façades cannot be modelled with MP damping with adequate confidence regarding consistency of input parameters and accuracy of results. Due to a major difference in computational runtime between MP and SP damping simulations, a practical relationship between the mass-proportional and the stiffness proportional damping parameters (α and β) was investigated. This attempt to correlate α and β does not enable the substitution of SP damping for MP damping simulations, but rather it allows simulated approximations to be generated with significantly less numerical effort as a precursor for the SP damping simulation that will produce simulations that are phenomenologically rigorous. To obtain the aforementioned correlation, free rocking simulations of single blocks which were found to provide a reasonable matching with experimental observations were parametrised using a range of differing geometries. Experimentally matched simulation results, using both MP and SP damping approaches, were also included to obtain a relationship between α and β. The combination of the results led to a point cloud with an observable trend that allowed a relationship between α and β to be established. As part of the study of MP damped rocking blocks, a correlation was obtained between block geometry and the bouncing phenomena occurring during free rocking, showing that bouncing increased with increasing slenderness angle η per R length (η/R), and that bouncing was almost non-existent for blocks with $\eta \approx 5°$. No bouncing was observed when using SP damping.

Even though computation runtime was high, SP damping simulations were proven to correctly simulate the rocking behaviour of different URM parts. In every experiment simulated, SP damping results were found to be consistent with variation in material properties. The formulation to obtain SP damping developed by DeJong[43] was observed to work

for the one-way bending walls that were simulated but resulted in an overdamped simulation for parapets. The non-matching of results for parapets indicates that the DeJong[43] formulation, while the best tool to use to date, needs further development. It was also highlighted that there is a need for additional research directed towards the development of a procedure to assess the damping parameters of DEM one-sided rocking blocks, in order to eliminate the trial and error procedures currently being used. Furthermore, future research is needed to address the disconnect between DEM rocking simulations that apply Rayleigh damping and analytical models where the coefficient of restitution is applied, and also to analyse whether the correlation obtained by Vlachakis et al.[51] is indeed applicable to DEM. Future investigations will also be devoted to understanding the role of overburden loads on the damped motion of rocking blocks. The simulations presented herein were performed using the software 3DEC, but it is expected that similar trends will be observed when using other software where DEM is utilised, similar to the application of rigid-body-spring models or the applied-element method.[72,73] In the reported study, masonry was used as the reference material because of the extensive amount of research devoted to this form of construction, but the conclusions drawn from simulations using rocking masonry blocks can also be applied to concrete rocking blocks (e.g., bridge piers, nuclear reactor shields, water tanks, historic monuments) or non-structural rocking apparatus (e.g., hospital equipment).

DATA AVAILABILITY STATEMENT

Some or all data, models, or code that support the findings of this study are available from the corresponding author upon reasonable request.

ACKNOWLEDGEMENTS

This project was (partially) supported by QuakeCoRE, a New Zealand Tertiary Education Commission-funded Centre. This is QuakeCoRE publication number 0674. The authors also gratefully acknowledge the software 3DEC provided by Itasca consulting group under the Itasca Educational Partnership program. Dr Marta Giaretton and Dr Omar AlShawa are gratefully acknowledged for kindly sharing the raw data to perform the simulations reported herein.

Open Access Funding provided by Universita degli Studi di Roma La Sapienza within the CRUI-CARE Agreement.

ORCID

Francisco Galvez https://orcid.org/0000-0002-8507-4281
Luigi Sorrentino https://orcid.org/0000-0003-1652-942X

REFERENCES

1. Nayeri SA. *Seismic Assessment of the Roman Temple in Évora, Portugal*. Universidade do Minho; 2012.
2. Zamani N, El Shamy U. Discrete-element method simulations of the response of soil-foundation-structure systems to multidirectional seismic motion. *Int J Geomech*. 2013;13(5):595-610.
3. Mehrotra A, DeJong M. The performance of slender monuments during the 2015 gorkha, Nepal, Earthquake. *Earthquake Spectra*. 2017;33(S1):S321-S343.
4. Erdogmus E, Pulatsu B, Can B, Ozkan K, Analysis of the last standing arch of the Roman Aqueduct at Blaundos. presented at: Proceedings of the Thirteenth North American Masonry Conference; 2019; Salt Lake City, Utah.
5. Malomo D, Mehrotra A, DeJong MJ. Distinct element modeling of the dynamic response of a rocking podium tested on a shake table. *Earthquake Eng Struct Dyn*. 2020;50(5):1469-1475.
6. Forgács T, Sarhosis V, Ádány S. Shakedown and dynamic behaviour of masonry arch railway bridges. *Eng Struct*. 2021:228.
7. Kim J, Lorenzoni F, Salvalaggio M, Valluzzi MR. Seismic vulnerability assessment of free-standing massive masonry columns by the 3D discrete element method. *Eng Struct*. 2021;246.
8. Cundall PA, A computer model for simulating progressive, large-scale movement in blocky rock system. Presented at: proceedings of the International Symposium on Rock Mechanics, 1971; 1971 1971; Nancy, France. https://ci.nii.ac.jp/naid/10018723276/en/
9. Cundall PA, Hart RD, Development of generalized 2d and 3d distinct element programs for modeling jointed rock. 1985.
10. Šmilauer V, Catalano E, Chareyre B, et al. *Yade Documentation*. 2nd ed. The Yade Project; 2015. http://yade-dem.org/doc/.
11. 3DEC (3-Dimensional distinct element code). Version 5.2. 2013.
12. Lemos JV. Discrete element modeling of the seismic behavior of masonry construction. *Buildings*. 2019;9(2):43.
13. Papantonopoulos CL, The earthquake resistance of ancient columns: a numerical perspective developed at the classical temple of apollo epikourios. Presented at: structural studies, repairs and maintenance of historical buildings - STREMAH V; 1997;
14. Zhong X, Sun W. An adaptive reduced-dimensional discrete element model for dynamic responses of granular materials with high-frequency noises. *Int J Multiscale Comput Eng*. 2018;16(4):345-366.
15. Lemos JV, Discrete element modelling of historical structures. Presented at: Proc Int Conf New Technologies in Structural Engineering; 1996; LNEC, Lisbon.

16. Lemos JV, Discrete element modelling of the seismic behaviour of stone masonry arches. presented at: Proc 4rd Int Symp Num Methods Structural Masonry - STRUMAS IV; 1997; Florence, Italy.
17. Papastamatiou D, Psycharis IN. Seismic response of classical monuments—a numerical perspective developed at the Temple of Apollo in Bassae, Greece. *Terra Nova*. 1993;5:591-601.
18. Mordanova A, de Felice G, Is seismic damage the reason for the Stern buttress of the Colosseum? Presented at: 6th International Conference: YOCOCU, Youth in Conservation of Cultural Heritage; May 22-26 2018 2018; Matera, Italy.
19. Galvez F, Giaretton M, Abeling S, Ingham JM, Dizhur D, Discrete element modeling of a two storey unreinforced masonry scaled model. Presented at: 16th European Conference on Earthquake Engineering; 18-21, June 2018; Thessaloniki, Greece.
20. Pulatsu B, Gencer F, Erdogmus E. Study of the effect of construction techniques on the seismic capacity of ancient dry-joint masonry towers through DEM. *Eur J Environ Civ Eng*. 2020:1-18.
21. Meriggi P, de Felice G, De Santis S, Gobbin F, Mordanova A, Pantò B. Distinct element modelling of masonry walls under out-of-plane seismic loading. *Int J Archit Heritage*. 2019;13(7):1110-1123.
22. Lemos JV, Campos Costa A. Simulation of shake table tests on out-of-plane masonry buildings. Part (V): discrete element approach. *Int J Archit Heritage*. 2017;11(1):117-124.
23. Lourenço PB. Computations on historic masonry structures. *Prog Struct Mater Eng*. 2002;4(3):301-319.
24. Psycharis IN, Drougas A, Daisou M. *Seismic behaviour of the walls of the parthenon a numerical study*. Computational Methods in Earthquake Engineering. 2011:21.
25. Psycharis IN, Papastamatiou DY. Alexandris AP. Parametric investigation of the stability of classical columns under harmonic and earthquake excitations. *Earthquake Eng Struct Dyn*. 2000;29:1093-1109.
26. Papantonopoulos C, Psycharis IN, Papastamatiou DY, Lemos JV, Mouzakis HP. Numerical prediction of the earthquake response of classical columns using the distinct element method. *Earthquake Eng Struct Dyn*. 2002;31(9):1699-1717.
27. Sarhosis V, Baraldi D, Lemos JV, Milani G. Dynamic behaviour of ancient freestanding multi-drum and monolithic columns subjected to horizontal and vertical excitations. *Soil Dyn Earthquake Eng*. 2019;120:39-57.
28. Godio M, Beyer K. Evaluation of force-based and displacement-based out-of-plane seismic assessment methods for unreinforced masonry walls through refined model simulations. *Earthquake Eng Struct Dyn*. 2018;48:454.
29. Mehrotra A, DeJong MJ. A methodology to account for interface flexibility and crushing effects in multi-block masonry collapse mechanisms. *Meccanica*. 2020;55(6):1237-1261.
30. Malomo D, DeJong MJ, Penna A. Distinct element modelling of the in-plane cyclic response of URM walls subjected to shear-compression. *Earthquake Eng Struct Dyn*. 2019;48(12):1322-1344.
31. Lipo B, de Felice G, Seismic resilience of masonry walls rocking on elastic foundation. Presented at: 16th World Conference on Earthquake, 16WCEE 2017 January 9th to 13th 2017 2017; Santiago, Chile,.
32. ElGawady MA, Ma Q, Butterworth JW, Ingham J. Effects of interface material on the performance of free rocking blocks. *Earthquake Eng Struct Dyn*. 2011;40(4):375-392.
33. Li X, Basic problems of the explicit numerical method for analyzing the earthquake response of inhomogeneous local site. Presented at: Eleventh World Conference on Earthquake Engineering; 1996;
34. Nsiampa N, Ponthot J-P, Noels L. Comparative study of numerical explicit schemes for impact problems. *Int J Impact Eng*. 2008;35:1688-1694.
35. Hulbert GM, Chung J. Explicit time integration algorithms for structural dynamics with optimal numerical dissipation. *Comput Meth Appl Mech Eng*. 1996:137.
36. Meyer P, Ochsendorf J, Germaine J, Kausel E, The impact of high-frequency/low-energy seismic waves on unreinforced masonry. *Earthquake Spectra*. 2007;23(1):77-94. https://doi.org/10.1193/1.2431211
37. Dimitri R, De Lorenzis L, Zavarise G, Numerical study on the dynamic behavior of masonry columns and arches on buttresses with the discrete element method. *Eng Struct*. 2011;33(12):3172-3188. https://doi.org/10.1016/j.engstruct.2011.08.018
38. Lorig LJ, Hart RD, Block dynamics modeling in support of seismic design. Presented at: dynamic analysis and design considerations for high-level nuclear waste repositories; 1993; New York.
39. Jing L, Stephansson O. *Explicit discrete element method for block systems—the distinct element method. Fundamentals of discrete element methods for rock engineering*. Elsevier; 2007:235-316.
40. Zhang H, Brogliato B, Liu C. Dynamics of planar rocking-blocks with Coulomb friction and unilateral constraints: comparisons between experimental and numerical data. *Multibody System Dynamics*. 2014;32(1):1-25.
41. Ma QT, The mechanics of rocking structures subjected to ground motion. PhD Dissertation. University of Auckland; 2010.
42. Scalia A, Sumbatyan MA. Slide rotation of rigid bodies subjected to a horizontal ground motion. *Earthquake Eng Struct Dyn*. 1996;25:1139-1149.
43. DeJong MJ, Seismic assessment strategies for masonry structures. PhD Dissertation. Massachusetts Institute of Technology; 2009.
44. Çaktı E, Saygılı Ö, Lemos JV, Oliveira CS. Discrete element modeling of a scaled masonry structure and its validation. *Eng Struct*. 2016;126:224-236.
45. Psycharis IN, Lemos JV, Papastamatiou DY, Zambas C, Papantonopoulos C. Numerical study of the seismic behaviour of a part of the Parthenon Pronaos. *Earthquake Eng Struct Dyn*. 2003;32(13):2063-2084.
46. Çaktı E, Saygılı Ö, Lemos JV, Oliveira CS. Nonlinear dynamic response of stone masonry minarets under harmonic excitation. *Bull Earthquake Eng*. 2020.

47. Vamvatsikos D, Cornell CA. Incremental dynamic analysis. *Earthquake Eng Struct Dyn*. 2002;31(3):491-514.
48. Psycharis IN. A probe into the seismic history of athens, Greece from the current state of a classical monument. *Earthquake Spectra*. 2007;23(2):393-415.
49. DeJong MJ, Vibert C. Seismic response of stone masonry spires: computational and experimental modeling. *Eng Struct*. 2012;40:566-574.
50. Kalliontzis D, Sritharan S. Characterizing dynamic decay of motion of free-standing rocking members. *Earthquake Spectra*. 2018;34(2):843-866.
51. Vlachakis G, Giouvanidis AI, Mehrotra A, Lourenço PB. Numerical block-based simulation of rocking structures using a novel universal viscous damping model. *J Eng Mech*. 2021;147(11).
52. Peña F, Prieto F, Lourenço PB, Campos Costa A, Lemos JV. On the dynamics of rocking motion of single rigid-block structures. *Earthquake Eng Struct Dyn*. 2007;36(15):2383-2399.
53. Tomassetti U, Graziotti F, Sorrentino L, Penna A. Modelling rocking response via equivalent viscous damping. *Earthquake Eng Struct Dyn*. 2019.
54. Bathe KJ, Wilson EL. *Numerical methods in finite element analysis*. Prentice-Hall; 1976.
55. Lam NTK, Griffith M. Time–history analysis of URM walls in out-of-plane flexure. *Eng Struct*. 2003;25(6):743-754.
56. Chopra AK. *Dynamics of structures. Theory and applications to earthquake engineering*. 4 ed. 1995.
57. Belytschko T. An overview of semidiscretization and time integration procedures. *Computational methods for transient analysis*. Elsevier Science Publishers BV; 1983:1-65.
58. Shawa OA, de Felice G, Mauro A, Sorrentino L. Out-of-plane seismic behaviour of rocking masonry walls. *J Earthq Eng Struct Dyn*. 2012;5(2):253-271.
59. Lipscombe PR, Pellegrino S. Free rocking of prismatic blocks. *J Eng Mech*. 1993;119(7):1387-1410.
60. Galvez F, Segatta S, Giaretton M, Walsh KQ, Giongo I, Dizhur D, FE and DE modelling of out-of-plane two-way bending behaviour of unreinforced masonry walls. Presented at: 16th European Conference on Earthquake Engineering; 2018; Thessaloniki, Greece.
61. Tondelli M, Beyer K, DeJong M. Influence of boundary conditions on the out-of-plane response of brick masonry walls in buildings with RC slabs. *Earthquake Eng Struct Dyn*. 2016;45(8):1337-1356.
62. Pulatsu B, Erdogmus E, Lourenço PB, Quey R. Simulation of uniaxial tensile behavior of quasi-brittle materials using softening contact models in DEM. *Int J Fract*. 2019.
63. Sorrentino L, AlShawa O, Decanini LD. The relevance of energy damping in unreinforced masonry rocking mechanisms. Experimental and analytic investigations. *Bull Earthquake Eng*. 2011;9(5):1617-1642.
64. Housner GW. The behavior of inverted pendulum structures during earthquakes. *Bull Seismol Soc Am*. 1963;53(2):403-417s.
65. Pulatsu B, Bretas EM, Lourenco PB. Discrete element modeling of masonry structures: validation and application. *Earthq Struct*. 2016;11(4):563-582.
66. Godio M, Stefanou I, Sab K. Effects of the dilatancy of joints and of the size of the building blocks on the mechanical behavior of masonry structures. *Meccanica*. 2018;53:1629-1643.
67. Lemos JV. Modelling the dynamics of masonry structures with discrete elements. *Open Constr Build Technol J* . 2016;10(2: M3):210-219.
68. Lemos JV. Contact representation in rigid block models of masonry. *Int J Mason Res Innov*. 2017;2(4):321-334.
69. Giaretton M, Dizhur D, Ingham JM, Dynamic testing of as-built clay brick unreinforced masonry parapets. *Eng Struct*. 2016;127:676-685. https://doi.org/10.1016/j.engstruct.2016.09.016
70. Griffith MC, Lam NTK, Wilson JL, Doherty K. Experimental investigation of unreinforced brick masonry walls in flexure. *J Struct Eng*. 2004;130(3):423-432.
71. Godio M, Beyer K. Analytical model for the out-of-plane response of vertically spanning unreinforced masonry walls. *Earthquake Eng Struct Dyn*. 2017;46(15):2757-2776.
72. D'Altri AM, Sarhosis V, Milani G, et al. Modeling strategies for the computational analysis of unreinforced masonry structures: review and classification. *Arch Comput Meth Eng*. 2019.
73. Malomo D, Pinho R, Penna A. Applied element modelling of the dynamic response of a full-scale clay brick masonry building specimen with flexible diaphragms. *Int J Archit Heritage*. 2019:1-18.

How to cite this article: Galvez F, Sorrentino L, Dizhur D, Ingham JM. Damping considerations for rocking block dynamics using the discrete element method. *Earthquake Engng Struct Dyn*. 2022;51:935–957. https://doi.org/10.1002/eqe.3598